Effect of Copper Contamination at the Cathode in Cu-Cl Electrolyzers for Hydrogen Production

by

Sydney L. Cobourn

A thesis submitted to the
School of Graduate and Postdoctoral Studies in partial
fulfillment of the requirements for the degree of

Master of Science in Materials Science

Faculty of Science

University of Ontario Institute of Technology (Ontario Tech University)

Oshawa, Ontario, Canada

April 2020

THESIS EXAMINATION INFORMATION

Submitted by: **Sydney L. Cobourn**

Master of Science in Materials Science

Thesis title: Effect of Copper Contamination at the Cathode in Cu-Cl Electrolyzers

An oral defense of this thesis took place on February 26, 2020 in front of the following examining committee:

Examining Committee:

Chair of Examining Committee	Dr. Franco Gaspari
Research Supervisor	Dr. E. Bradley Easton
Examining Committee Member	Dr. Brian Ikeda
Examining Committee Member	Dr. Aaron Slepkov
Thesis Examiner	Dr. Jean-Paul Desaulniers

The above committee determined that the thesis is acceptable in form and content and that a satisfactory knowledge of the field covered by the thesis was demonstrated by the candidate during an oral examination. A signed copy of the Certificate of Approval is available from the School of Graduate and Postdoctoral Studies.

AUTHOR'S DECLARATION

I hereby declare that this thesis consists of original work of which I have authored. This is a true copy of the thesis, including any required final revisions, as accepted by my examiners.

I authorize the University of Ontario Institute of Technology (Ontario Tech University) to lend this thesis to other institutions or individuals for the purpose of scholarly research. I further authorize University of Ontario Institute of Technology (Ontario Tech University) to reproduce this thesis by photocopying or by other means, in total or in part, at the request of other institutions or individuals for the purpose of scholarly research. I understand that my thesis will be made electronically available to the public.

_____ Sydney L. Cobourn

STATEMENT OF CONTRIBUTIONS

Part of the work described in Chapter 4 has been published as:

S.L. Cobourn, E.B. Easton, “The effect of copper contamination at the cathode of CuCl/HCl electrolyzers", *International Journal of Hydrogen Energy, 42 (*2017) 28157 - 28163. doi:10.1016/j.ijhydene.2017.09.142

I performed all electrochemical measurements as well as cell construction/up-keep. I was also responsible for the majority of the writing of the manuscript.

CONTENTS

ABSTRACT

In this work the effects of copper contamination on the coulombic and voltage efficiency of the hydrogen evolution reaction (HER) via the Cu-Cl thermochemical cycle are investigated. A novel proton pump configuration was employed, which allowed for the copper concentration at the cathode to be controlled. A variety of electrochemical tests were performed to evaluate the effect of copper on the system. The purpose of this research project was to determine the threshold for copper contamination at the cathode in these Cu-Cl/HCl electrolyzers. Results of electrochemical test show that there is a significant increase in overpotential and a negative impact on HER kinetics with increasing copper concentration in both a chloride rich and chloride-free environment. In both media the Coulombic efficiency remains constant regardless of the concentration of copper in the catholyte. Results suggest that when the concentration of copper is greater than 5 ppm, the effects of copper contamination becomes significant.

Keywords: Hydrogen, Cu-Cl/HCl thermochemical cycle, proton-pump, electrolysis.

ACKNOWLEDGEMENTS

My Journey at the University of Ontario Institute of Technology (UOIT) has been nothing short of life changing. I have met some of the most interesting people, learned some of the most interesting things and all in all, have been shaped into an interesting person as a result. I could not imagine being anyone else than the person I am today and UOIT has played an incredibly important role in shaping that person. I would like to thank with the greatest sincerity, the institution as a whole for giving me the opportunity to become the person I am proud to be today.

There were a number of colleagues that were not specifically involved in the graduate studies program that extended their resources and insight towards my work that contributed to my work significantly. I would like to thank Michael Allison, Clayton Jakins, Genevieve Barns, and last but definitely not least, Dr. Richard Bartholomew. These fine scientists were present and active throughout not only my time as an undergraduate, but also helped me immensely throughout my graduate studies. Their help and support could not have been replaced and I could not imagine being where I am without their continuous efforts to better my quality of education.

I would like to extend a special thank you to my supervisor, Dr. E. Bradley Easton. He was supportive, encouraging and insightful in every aspect of his guidance throughout this journey. Even when I fell on hard times, he was compassionate, caring and had my back through all of it. Another supervisor may not have done the same, and I feel blessed to have had him as my mentor. My educational goals would have never been accomplished without his constant faith in my abilities. I feel honored to have studied under such an accomplished, compassionate professional.

The Easton lab group including all members that have come and gone in my time here, I also have a deep appreciation for these people I am happy to call friends after our time together and many were fantastic mentors and teachers as well. As they say I takes a village and it could not be more of a true statement. Without the help of my lab mates, I would have been lost and my learning experience would have been sub-par in comparison to the one I got. These people were essential to the success of my degree and I have so much respect for all of them. They will make the scientific community a more challenging place to be a part of.

Finally, I would like to thank my family. My parents have always been there to support me throughout all of the struggles I endured in both my undergraduate and graduate studies. They have celebrated my accomplishments and comforted me during times I have failed. This group of people have been my support system throughout my educational journey, and I cannot express how grateful I am to have had them here for me. I would like to dedicate this work to my mother, Linda Cobourn, who has been my best friend for as long as I can remember. She always makes sure I'm fed, happy, safe and is completely on my case when I start to waver. Without her I would never have made it to where I am today. I owe her more than she will ever know.

Thank you to all of the people who made my success as a graduate student possible. It was not solely an effort on my part, but an effort put forth by many individuals. This is not an accomplishment that I consider my own, but an accomplishment I consider belonging to all of those who believed in me enough to put up with me through all the struggles I endured. I am forever grateful.

LIST OF TABLES

LIST OF FIGURES

COMMON ABBREVIATIONS

ΔG° – Standard Gibbs free energy change

μL- Microliter

μm- Micrometer

η- Overpotential

A- Ampere

CE- Counter electrode

CV- Cyclic voltammetry

ECSA- Electrochemically active surface area

GHG- Greenhouse gas

HER- Hydrogen evolution reaction

$Hg/HgSO_4$- Mercury/mercury-sulfate electrode

I- Current

L- Liter

LSV- Linear sweep voltammetry

M- Molar (mol/L)

mA- Milliampere

min- Minute

mm- Millimeter

mV- millivolt

n- Number of moles of a chemical species/electron

nA- Nanoampere

P- Pressure

PEM- Polymer Electrolyte Membrane/Proton Exchange Membrane

ppm- Parts per million

Pt/C- Platinum on carbon

RE- Reference electrode

RHE- Reversible hydrogen electrode

s- Second

SHE- Standard hydrogen electrode

SOEC- Solid Oxide Electrolytic Cell

SRP- Standard reduction potential (vs. SHE)

STP- Standard temperature and pressure (273 K, 1 bar)

T- Temperature

UPD- Underpotential deposition

UV-vis- UV-Visible Spectroscopy

V- Voltage

V- Volume

WE- Working electrode

CHAPTER 1: HYDROGEN AS A CLEAN ENERGY CARRIER

1.1 Hydrogen as a Clean Energy Carrier

Currently the majority of the world's energy needs are met by exploiting fossil fuels. These are non-renewable resources that are depleting rapidly[1-5]. The use of these fuel sources results in the release of greenhouse gases (GHG) into the atmosphere[6]. These are gaseous chemical species (e.g. CO_2, CH_4, NO_X,) that absorb light reflected from the earth's surface which occur in the infrared wavelength region. These wavelengths are absorbed in the form of heat. This heat absorption results in an overall increase in global temperature and in turn a change in climate patterns[7-10]. For the world to continue to meet its energy needs while continuing to preserve the planet's integrity, it is essential to find a method of meeting our energy needs that does not result in the release of detrimental greenhouse gases into the atmosphere.

There are two types of energy which are termed primary and secondary energy sources. Primary energy sources include raw materials that can be converted into energy carriers such as fossil fuels, or renewable energy sources that transfer energy rather than come from the irreversible transformation of a material. These types of primary energy sources include hydroelectric, solar and wind power. Secondary energy sources result in the production of energy carriers and must be produced from primary energy sources. Examples of secondary energy sources include electricity and hydrogen gas[7,11].

This suggests that the most appropriate means of preventing the greenhouse gas emissions is to employ a fuel that is free of hydrocarbons. One potential source that has gained increasing interest over the years in molecular hydrogen[12]. With the development of hydrogen fuel cell technology, this species has been recognized as one of the most promising clean energy carriers to date[2,9,10,13-18]. The reaction that takes place within a hydrogen fuel cell results only in the production of liquid water, meaning there is no inherent pollution directly associated with the use

of this chemical as a fuel source. Hydrogen is superior to many of the non-renewable fuel sources we currently employ as it has a much higher energy density, can be converted to and from electricity with relative ease, and can be stored as a solid, liquid or gas. Molecular hydrogen has been widely recognized as the fuel of the future.

Currently, we obtain approximately 96% of the world's molecular hydrogen from the reforming of fossil fuels. These processes ultimately result in side products that are considered greenhouse gases[2,9,19,11,15,17,18]. One example of this is the steam reforming of methane gas. This process first involves two reforming reactions and the water-gas shift reaction which are shown in Equations 1-2 and 3, respectively. These reactions are typically performed over a nickel catalyst at high temperatures[20]. The resources employed to produce molecular hydrogen to date can be seen in Figure 1.1. These processes essentially cancel out the environmental benefits associated with employing hydrogen as a clean energy carrier. In order to fully maximize the clean energy carrier which is hydrogen gas, it is first necessary to develop a GHG neutral method of production.

$$CH_4 + H_2O \rightarrow CO + 3H_2 \qquad (Eq.1)$$

$$CH_4 + 2H_2O \rightarrow CO_2 + 4H_2 \qquad (Eq.2)$$

$$CO + H_2O \leftrightarrow CO_2 + H_2 \qquad (Eq.3)$$

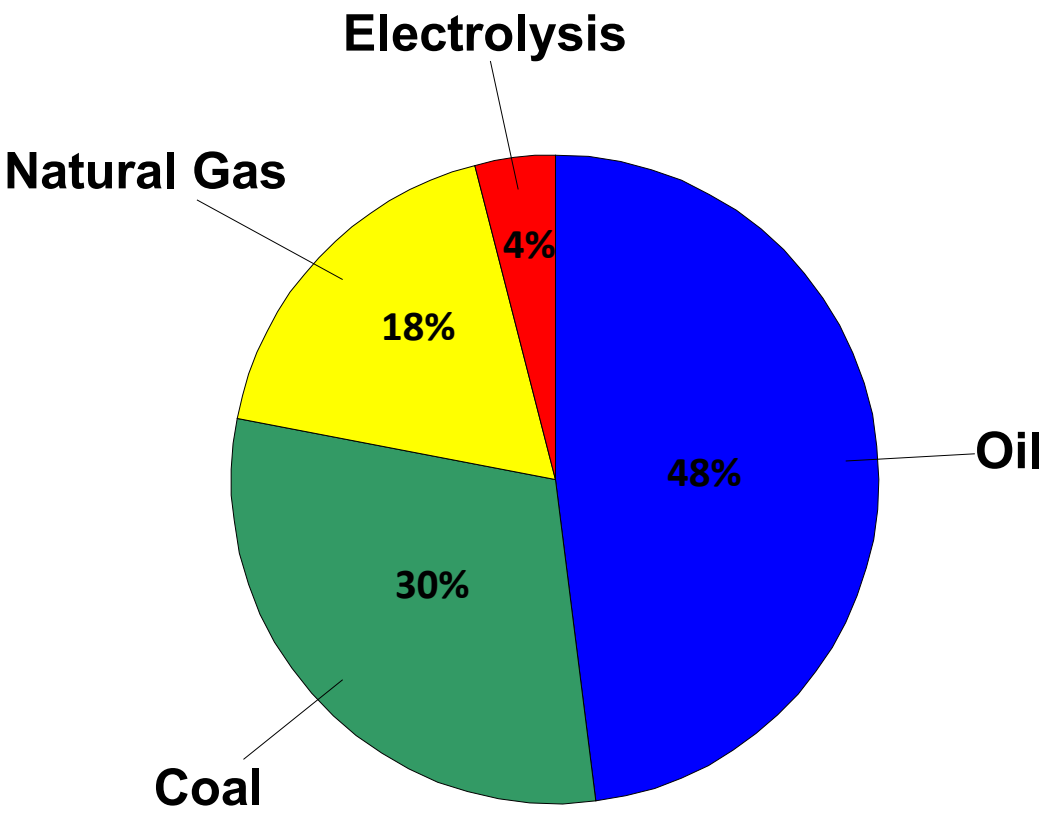

Figure 1.1: Current methods used for the global production of molecular hydrogen[7,17,21].

1.1.1 Electrolysis

Electrolysis is a process by which a chemical compound is decomposed due to the application of electrical potential energy. Water electrolysis has many benefits including simplicity of the reaction, high purity product, no pollutants and availability. This is an energy intensive process requiring an applied potential of at least 1.23 V and Gibbs free energy of 237.2 kJ/mol[14,12].

This process can be performed in either an alkaline or acidic media, each of which offer unique benefits and drawbacks. Half reactions and associated reduction potentials can be found in Tables 1.1 and 1.2. High energy requirements are the main reason that electrolysis has not yet

been implemented as a large-scale method of hydrogen production. The reaction equation for this process can been seen in Equation 4. For electrolysis to become a practical method of producing hydrogen gas on a large scale, it is first necessary to find a method of producing this chemical species that is both carbon neutral and energy efficient.

$$H_2O \xrightarrow{1.23\,V} \frac{1}{2}O_2 + H_2 \qquad \Delta G = 237\frac{kJ}{mol} \qquad (Eq.4)$$

Table 1.1: Half-cell reactions for water electrolysis performed in an acidic media[22]

Reaction	Equation	E° (V)
Cathode	$2H^+ + 2e \rightarrow H_2$	0
Anode	$H_2O \rightarrow 1/2O_2 + 2H^+$	1.23

Table 1.2: Half-cell reactions for water electrolysis performed in an alkaline media[22]

Reaction	Equation	E° (V)
Cathode	$2H_2O + 2e \rightarrow\ H_2 + 2OH^-$	-0.83
Anode	$2OH^- \rightarrow\ H_2O + 1/2O_2$	0.4

1.1.2 Alkaline Electrolysis Cells

Water electrolysis can be performed in an acidic media. This type of cell has many benefits as well as a number of drawbacks associated with the technology. This version of an electrolytic cell operates using two electrodes, the cathode which is referred to as the positive electrode, and the anode, which is the negative electrode. These electrodes are separated by a diaphragm that serves the main purpose of gas separation for safety and efficiency. The electrodes are submersed in a liquid electrolyte containing approximately 20-30% KOH[23]. A diagram depicting a typical alkaline electrolytic cell can be seen in Figure 1.2.

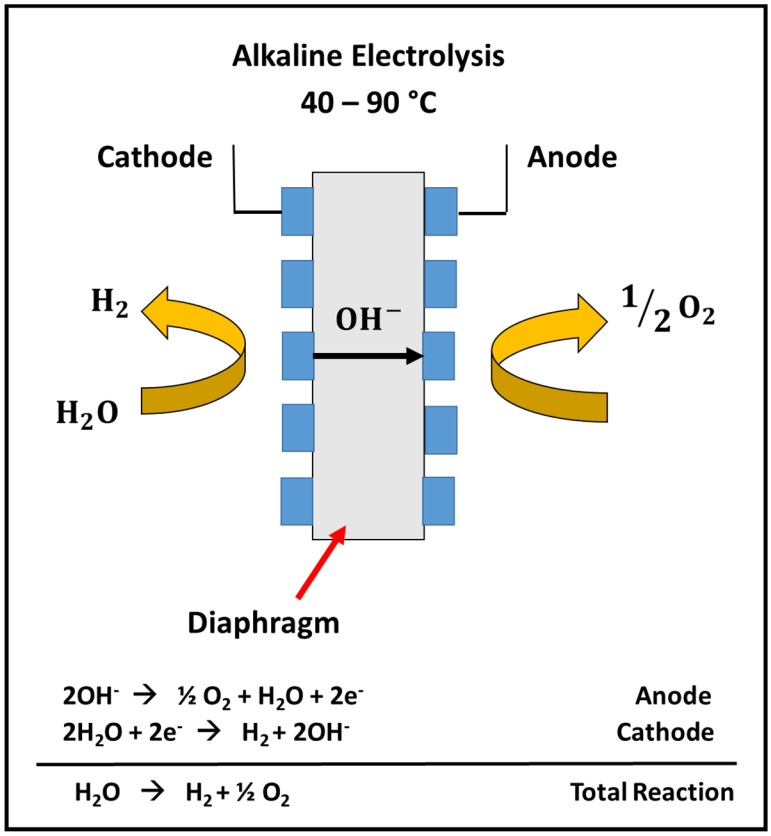

Figure 1.2: Diagram of an alkaline electrolysis cell[23].

There are several disadvantages associated with producing hydrogen in an alkaline electrolytic cell. The first is the fact that this technology cannot handle a partial load safely[23]. When the load of the system is less than 40% the rate of oxygen production significantly decreases which results in an increased amount of hydrogen at the cathode. If the H_2 concentration reaches a value greater than 4%, then the system is no longer considered safe as this is the lower explosion limit of hydrogen gas[23]. The second drawback associated with alkaline electrolytic cells is the limited maximum current densities that are possible to achieve. Both the liquid electrolyte and the diaphragm component of the system impart resistance. This resistance ultimately results in Ohmic loses and in turn decreased efficiency of the electrolysis process. Optimizing these components by employing the least resistive materials and solutions is a significant area of interest. Thirdly, alkaline electrolytic cells suffer from low operating pressure. This phenomenon is also due to the effects of employing a liquid electrolyte and results in bulky stack designs[23].

1.1.3 Polymer Electrolyte Membrane Fuel Cells (PEMFC's)

Polymer electrolyte membrane (PEM) cells employ a solid polymer electrolyte called Nafion®. The structure of this material can be seen in Figure 1.3. This is a sulfonated tetrafluoroethylene polymer having a thickness between 20-300 μm. These thin membranes are negatively charged and therefore act as an efficient cation exchange membrane, allowing protons to cross over from the anode to the cathode where they are reduced to form hydrogen gas. These types of cells offer a number of benefits including low gas crossover, high pressure operation and

allow for the development of compact systems. These systems have their own particular set of advantages and disadvantages in terms of effectiveness for the electrolysis process.

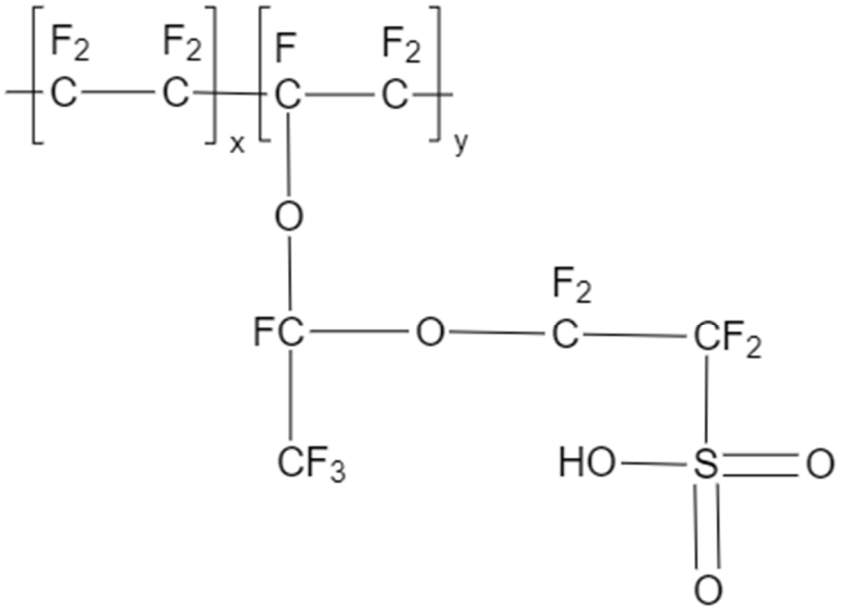

Figure 1.3: Chemical structure of Nafion®

PEM electrolysis cells have the benefit of being able to operate at high current densities, which is not the case of the well-studied alkaline electrolysis system. Current densities as high as 2 A/cm^2 have been observed. As in any electrochemical system, the maximum observable current density is limited in part by Ohmic losses. Employing thin membranes with high proton conductivity decreases these ohmic losses in comparison to a system that employs a liquid electrolyte. Another advantage to PEM cell technology is the low rate of gas crossover. Unlike the alkaline electrolysis systems developed to date, PEM cells can operate under a wide range of load

ranges. Alkaline fuels cells as discussed earlier in this section, suffer from low oxygen generation when the load is less than 40% resulting in an increased concentration of hydrogen gas at the cathode, which compromises the safety of the set-up and risks the possibility of an explosion. Protons are able to be transported quickly across the membrane allowing the system to respond nearly immediately to the change in applied voltage. The lack of crossover also results in a high level of purity of the H_2 produced during the reaction. Ultimately another advantage to employing a solid polymer electrolyte such as Nafion is ability to develop a compact cell design. Without the need to incorporate liquid electrolytes, the cell stacks needed for large scale hydrogen production are more practical, mirroring the SOEC type of systems. There have been commercial models developed employing a PEM configuration which have shown to be able to operate at pressures up to 350 bars. When electrolytic cells are able to run at such high pressures there is a beneficial phenomenon known as electrochemical compression. This refers to the fact that hydrogen is delivered to the cathode at high rates when the pressure is a great deal higher than standard temperature and pressure (STP; 273 K, 1 bar)[23]. A diagram of a typical PEM cell can be seen in Figure 1.4.

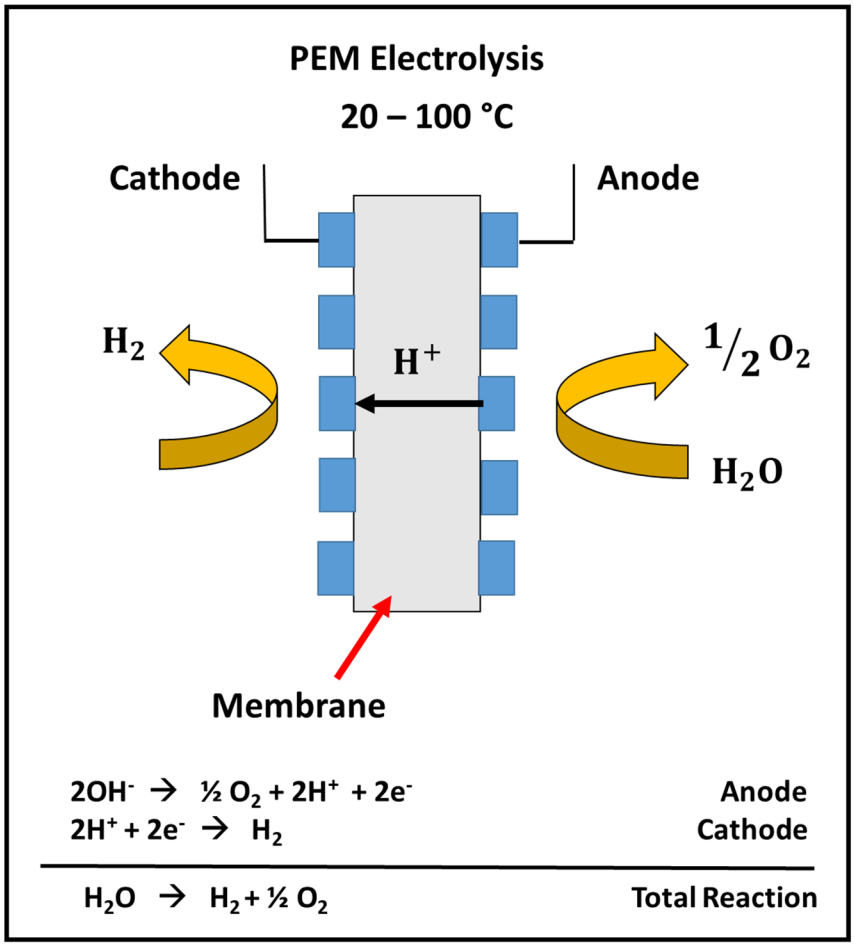

Figure 1.4: Diagram of a typical PEM electrolysis cell[23].

1.1.4 Solid Oxide Electrochemical Cells (SOEC's)

This particular type of electrolysis cell has intrigued scientists in recent decades as they have the ability to convert electrical energy to chemical energy and, therefore, produce molecular hydrogen with great efficiency. There have been reports in literature of SOEC's being operated with current densities of 0.3 A/cm^2 having 100% faradaic efficiency, with the applied voltage being approximately only 1 V. The main drawback associated with this particular type of electrolytic cell is the durability of the ceramic materials employed. It is essential that these

durability issues, as well as the ability of the materials to hold up under high temperature conditions, be improved for this type of technology to become a more practical option for large scale, long term clean hydrogen production[23].

1.2 The Cu-Cl Hybrid Thermochemical Cycle

1.2.1 Thermochemical Cycles

This particular type of electrolysis cell has intrigued scientists in recent decades as they have the ability to convert electrical energy to chemical energy and, therefore, produce molecular hydrogen with great efficiency. There have been reports in literature of SOEC's being operated with current densities of 0.3 A/cm^2 having 100% faradaic efficiency, with the applied voltage being approximately only 1 V. The main drawback associated with this particular type of electrolytic cell is the durability of the ceramic materials employed. It is essential that these durability issues, as well as the ability of the materials to hold up under high temperature conditions, be improved for this type of technology to become a more practical option for large scale, long term clean hydrogen production[23].

1.2.2 The Cu-Cl/HCl Thermochemical Cycle

The Cu-Cl thermochemical cycle is one of the most promising due to a number of factors. This particular cycle has considerably lower temperature requirements ($< 550℃$) in comparison to the other practical cycles[9,24-29]. Low temperature requirements also lead to lower maintenance costs as high temperatures result in increased strain on materials in large scale systems[30]. The Cu-Cl/HCl cycle has many benefits including inexpensive reactants, low instances of side reactions,

could be paired with generation IV super critical water-cooled reactors (SCWR's) and also has a significantly lower potential requirements than conventional electrolysis[19,31,27-28]. There are a number of variations of this cycle that can be employed in order to perform the water splitting reaction. The incorporation of an electrochemical step makes the process a hybrid thermochemical cycle. Tables 1.3 and 1.4 show the reaction equations involved as well as the temperature requirements for the 4 and 5 step Cu-Cl/HCl thermochemical cycle respectively. A diagram depicting the steps in the 3 step CuCl thermochemical cycle can be seen in Figure 1.5.

Table 1.3: Reactions occuring in the 5 step Cu-Cl thermochemical cycle[3]

Reaction equation	Temperature (℃)
$2CuCl_2(s) + H_2O(g) \rightarrow Cu_2OCl_2(s) + 2HCl(g)$	400
$Cu_2OCl_2(s) \rightarrow O_2(g) + 2CuCl(l)$	500
$4CuCl(aq) \rightarrow 2Cu(s) + 2CuCl_2(aq)$	25
$2Cu(s) + 2HCl(g) \rightarrow H_2(g) + 2CuCl(l)$	430
$CuCl_2(aq) \rightarrow CuCl_2(s)$	~100

Table 1.4: Reactions occuring in the 4 step Cu-Cl thermochemical cycle[3]

Reaction Equation	Temperature (°C)
$2CuCl(aq) + 2HCl(aq) \rightarrow 2H_2(g) + 2CuCl_2(aq)$	25
$Cu_2OCl_2(s) \rightarrow \frac{1}{2}O_2 + 2CuCl(l)$	500
$2CuCl_2(s) + H_2O(g) \rightarrow Cu_2OCl_2(s) + 2HCl$	400
$CuCl_2(aq) \rightarrow CuCl_2(s)$	~100

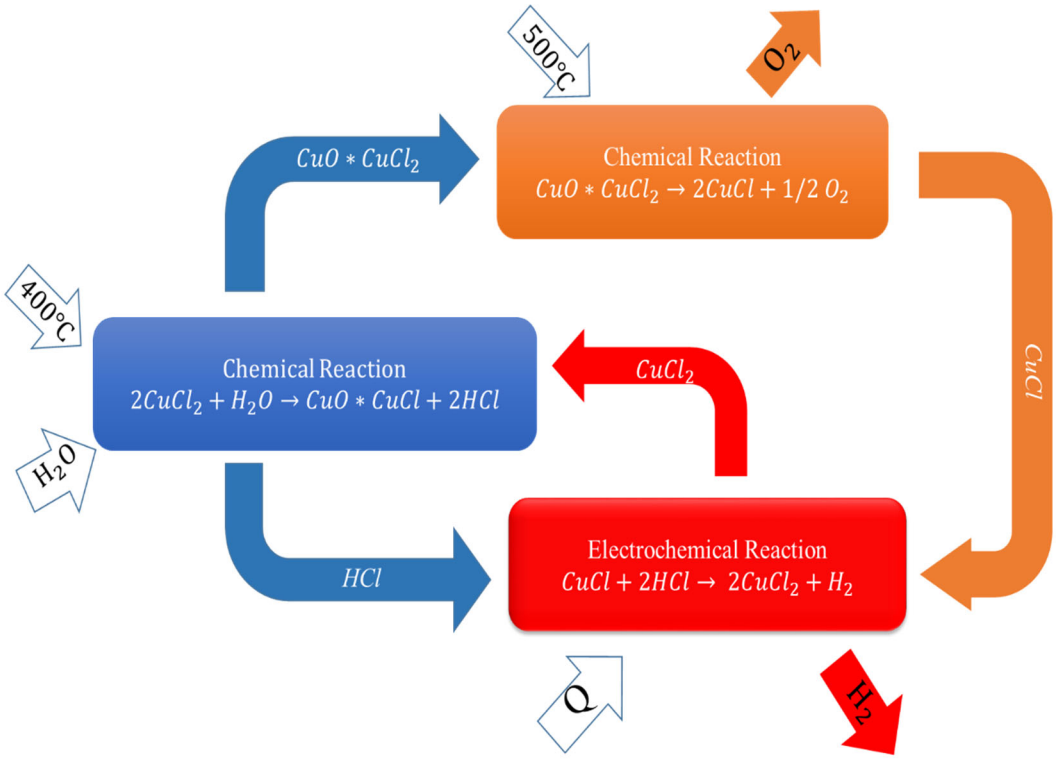

Figure 1.5: Reactions involved in the 3-step Cu-Cl/HCl hybrid thermochemical cycle.[32]

1.3 Copper Crossover

1.3.1 Effects of Copper Crossover

When copper crosses the proton exchange membrane from the anode compartment to the cathode compartment it then is able to plate onto the electrode surface. There is also a high probability of copper underpotential deposition taking place which increases the poisoning effects of the copper contaminants on the Pt electrode surface[33].

There are a number of different negative effects that surface poisoning can have on the electrolytic process. When there is a plating of the copper species onto the Pt active sites, these copper atoms must be removed first in order to expose these Pt catalytic sites for protons that will be converted to molecular hydrogen. The HER requires a potential of 0 V to occur. Due to the fact that the HER is a reductive process, any kinetic restraints are noted by a negative increase in the potential observed under the application of a constant current density. An increasingly negative voltage requirement would indicate increasingly poor kinetics occurring at the working electrode, which in this experimental procedure is the cathode and is responsible for hydrogen evolution. Blockage of the Pt active sites can also impact the hydrogen production efficiency as there are fewer catalytic sites for the HER to take place. If the number of catalytic sites is diminished, the reaction rate will in turn be decreased and with that the amount of molecular hydrogen that could potentially be produced. Another phenomenon that can occur in this system is known as copper underpotential deposition (UPD). UPD is characterized by the formation of a monolayer of a metallic species on a substrate of a different chemical species. This monolayer formation occurs at a potential positive of the Nernst potential[34]

There have been many projects spanning a wide range of modifications of many different components of the current Cu-Cl electrolysis cell designs. These include modifications of the

catalyst material, the gas diffusion layer (GDL), membrane materials, and much more. In this section, a number of different approaches to minimize copper crossover within Cu-Cl electrolysis cells are discussed and analyzed.

1.3.2 Studying Cathodic Effect of Copper Crossover

Copper concentration and speciation at the cathode are dictated by reactions occurring at the anode, as this compartment is the side of the cell that contains the copper source. Any copper present at the cathode is there only due to copper ion permeation through the cation exchange membrane. Copper can be present on the cathode side of the cell in three different forms, Cu^0, Cu^{1+} or Cu^{2+}. Relying on the anodic reactions provides no control over the amount of each copper species. This makes it extremely difficult to study the effects associate with cathodic copper contamination and determine a threshold concentration of contaminants that are acceptable before the system suffers a dramatic decrease in kinetic and Coulombic efficiency.

1.4 Motivation

There has been a significant amount of research devoted to studying this Cu-Cl hybrid thermochemical cycle for hydrogen production. The anodic reactions completely dictate the amount of free copper in the anolyte, and therefore the amount of positive copper ions that have the potential to cross the PEM. When in the presence of chloride ions, copper ions form negatively charged complexes that gain an increasing negative charge as the number of chloride ions present increases. This increases with an increase in the free chloride concentration, which is the results of increasing the acid concentration on this side of the cell. Due to the dependence of speciation

on these anodic reactions it is very difficult to observe the effects that free copper ions have on the cathode.

In this study, the effects of copper contamination at the cathode was examined using a novel proton-pump cell configuration, described in Chapter 2. Using this technique, we were able to carefully control the concentration of Cu^{2+} at the cathode thereby allowing us to completely ignore voltage losses due to the anodic reactions. This allows us to determine the amount of copper that can be tolerated at the cathode before poisoning dramatically affects the kinetic efficiency of the reaction. This technology is not only limited to the study of the HER reactions in presence of copper, but can be employed in studying the effects of other contaminants for PEM electrolysis technology.

CHAPTER 2: MATERIALS AND METHODS

2.1 Instrumentation and Reagents

All solutions of H_2SO_4, HCl and $HClO_4$ were prepared from reagent grade chemicals obtained from Sigma Aldrich. Stock solutions of Cu^{2+} were prepared from solid $CuSO_4$ obtained from Sigma Aldrich. 18 MΩ deionized water (DI) was used in all cases. Solutions were deaerated with nitrogen gas (99.998%) prior to performing electrochemical testing. For tests performed in proton mode, hydrogen gas (99.999%) humidified via bubbling through deionized water was employed at the anode. A Pine WaveDriver 20 biopotentiostat controlled using Aftermath software was used for all three electrode cell tests, and a Solartron 1286 potentiostat operated with Corrview software was employed for all experiments performed in the full cell. Humidified gas at the anode and catholyte solution in the full cell configuration was supplied to the cell via a duel channel peristaltic pump (Masterflex L/S Digital Drive Pump: RK-07523-80) at a rate of 60 mL/min.

2.2 Three Electrode Cell Experiments

Prior to performing tests in the full cell configuration, 3-electrode cell experiments were performed in the presence of copper in order to investigate the effects of copper contamination on the HER. These experiments provided proof of concept. Initially, a 3 mm planar Pt working electrode was employed as the working electrode. The electrode surface was polished with a 0.05 μm aluminum polish to ensure that were no contaminants present. The reference electrode (RE) used was an $Hg/HgSO_4$ which was calibrated and found to have a potential of 700 mV_{RHE}. The counter electrode employed for these tests was a Pt wire

Experiments were then performed in the same way with the working electrode being changed to a 0.071 cm^2 glassy carbon (GC) electrode coated with a 20% Pt/C ink. This working electrode better reflects the surface of the electrode used in the full cell. Catalyst ink was prepared

by combing 10 mg of 20% Pt/C (Premetek) with 200 µL of Isopropyl alcohol (Sigma Aldrich), 200 µL of deionized water (DI) and 100 µL of Nafion. The Ink solution was then sonicated for 1 hour. Following sonication 2 µL of ink was deposited onto the electrode surface, yielding a Pt loading of ca. 0.11 mg/cm^2. A photograph of the three electrode cell set-up can be seen in Figure 3.

There were a number of solutions prepared and tested during this set of experiments. The effect of the copper concentration, chloride concentration and pH were investigated using both the 3 mm planar Pt electrode and the Pt/C coated GC electrode. Initially the chloride concentration as well as the pH of the solution were held constant while the copper concentration was varied. This was achieved by keeping the concentration of the HCl media at 0.1 M. The effects of pH of the solution with constant copper concentration was examined by altering the molarity of HCl while maintaining a constant copper concentration. The HCl concentration was 0.1, 0.5 or 1 M during these tests and for each of the HCl solutions tested the copper concentration was also varied from 0-10 ppm as in previous tests.

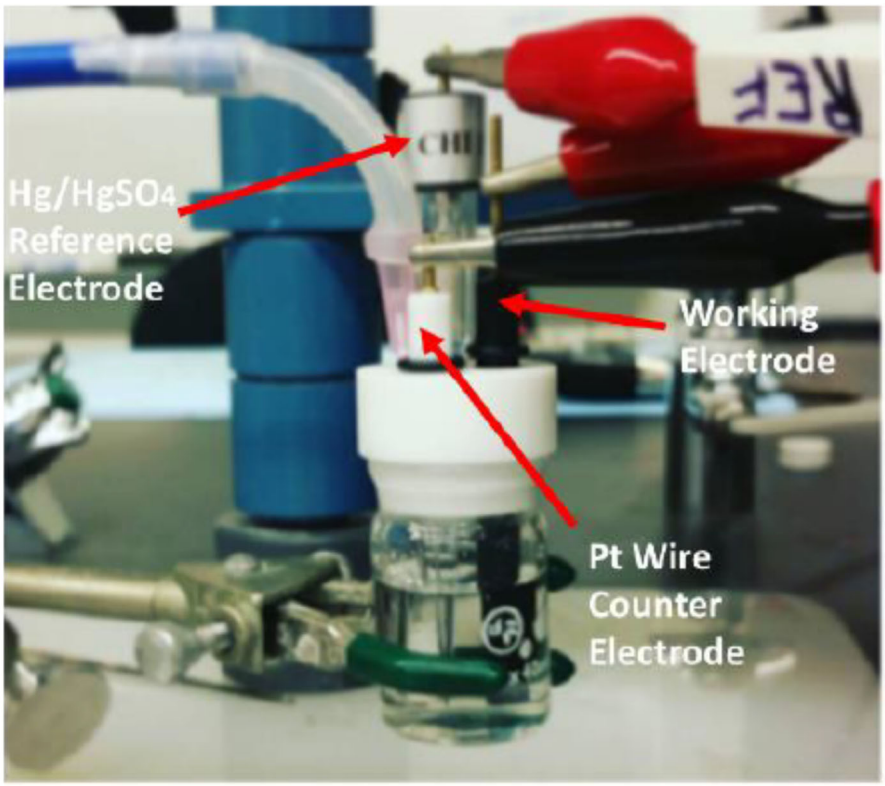

Figure 2.1: Three-Electrode cell set-up used for preliminary copper contamination experiments performed at 25 ℃

2.2.1 Electrochemical Tests

Before any electrochemical tests were performed the potential was cycled at a sweep rate of 150 mV/s for 30 cycles from 0.05-1.2 V_{RHE}. By cycling the potential in this way any adsorbed contaminants present on the electrode surface were removed. CV tests were then performed at a scan rate of 50 mV/s for a total of 4 cycles with the last cycle being reported in this thesis. Linear sweep voltammetry (LSV) experiments were performed directly following CV tests. The potential was scanned from 200 mV to – 200 mV at a scan rate of 5 mV/s. These electrochemical tests

allowed for the effect of copper contamination on the HER to be examined as the standard reduction potential of hydrogen is known to be 0 V.

2.3 Full Cell Experiments

2.3.1 Membrane Electrode Assembly (MEA) Preparation

Symmetrical MEA's were prepared by hot pressing two 5 cm^2 gas diffusion electrodes air brushed with Pt/C catalyst ink. The GDL used were carbon paper coated with a microporous layer (Ion Power Inc) and the final Pt loading was 0.2 mg/cm^2. Electrode materials were dried at 100 ℃ over night to ensure all water was removed. The anodic and cathodic electrodes were separated by a Nafion 115 (N115) membrane. The MEA was hot pressed at 100 °C for 90 seconds then placed in DI water and allowed to cool to room temperature prior to being placed in the electrolysis cell.

2.3.2 Cell Construction

The prepared MEA was placed in a conventional electrolysis cell. This component of the cell was place between two serpentine flow pattern bipolar graphite plates. The cell was held together using 4 bolts with a diameter of 3/8 of an inch that were hand tightened, and further tightened using to 50 in-lbs. Two 4 L glass tanks, which each possessed 4 ports, were used to hold the anolyte and the catholyte, which was varied based on the specific set of experiments. The electrolysis cell had both and import and export connection on both sides and the solutions that pass through the cell and were recycled to their original containers. A photograph of the electrolysis system can be seen in Figure 2.2.

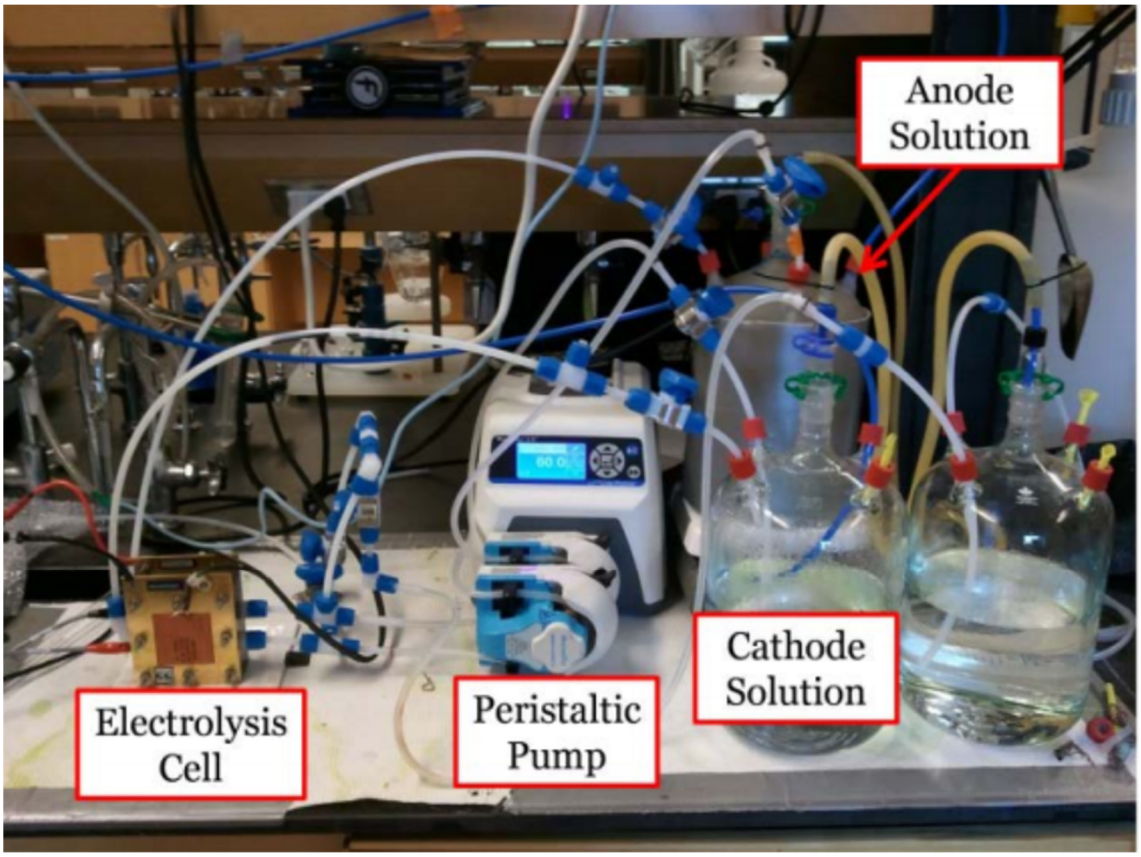

Figure 2.2: Photograph of electrolysis system constructed in house.

2.3.3.1 Proton-Pump Mode

Full cell experiments in this work were performed in a novel "proton-pump" configuration. In this set-up the anode feed is humidified hydrogen gas and the catholyte is an acidic solution. Molecular hydrogen is then oxidized to form protons that cross the PEM to the cathode compartment where they are reduced reforming molecular hydrogen. This causes the working electrode to also act as a RHE. Running this system in this way eliminates consideration associated with reactions occurring at the anode and allows for careful control the amount of copper at the cathode by spiking the catholyte. By performing experiments in the positive potential regime provides information about Pt surface health while running at negative potentials shows

the effects of copper contamination on the HER kinetics. A diagram of the electrolysis cell run in proton-pump mode can be seen in Figure 2.3.

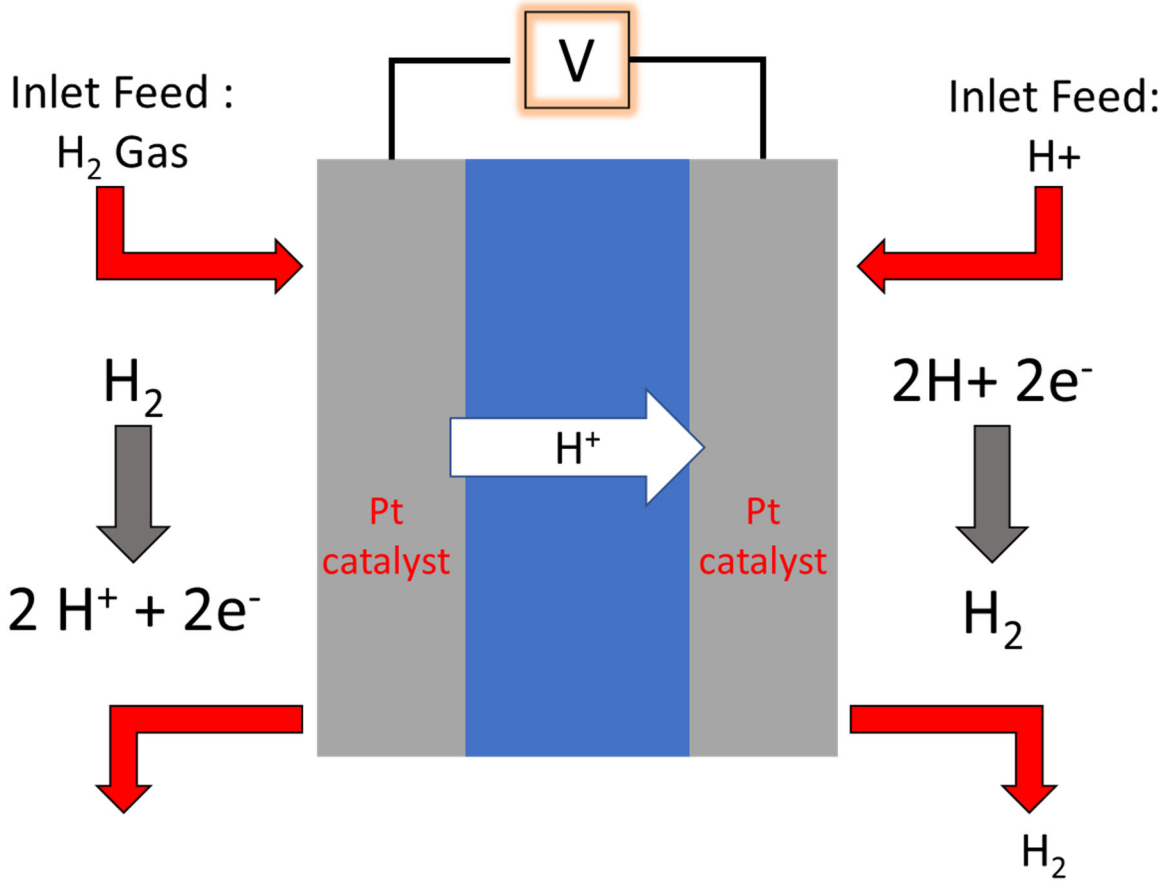

Figure 2.3: Diagram of the electrolysis cell run in proton pump mode.

2.3.3.2 Galvanostatic Hydrogen Production Experiments

Galvanostatic electrochemical tests differ from the methods described to this point as this type of experiment does not control the potential of the system, but the applied current instead. Therefore, if the current remains constant, as is the case in these particular experiments, the potential should remain constant as well if the resistance remains unchanged. Galvanostatic tests were performed at a constant current density of 300 mA/cm^2. This value was optimized through tests performed in the absence of copper. Optimization was necessary as current is a measure of the number of moles of electrons supplied to the system as a function of time and therefore directly related to the time required to produce the desired product, hydrogen gas. Currents ranging from 0.5-2 A were tested and it was found that applying a current of 1.5 A to the system allowed for a reasonable run time of 6 h while maintaining a stable signal.

Once the current density was optimized for system performance, experiments were performed with a catholyte having a concentration of 0.5 M H_2SO_4 in the absence of copper contaminants in order to obtain baseline data, The catholyte solution was then spiked with Cu^{2+} to produce a solution with final concentration from 1-10 ppm. For each experiment, the MEA used was freshly prepared and the system run for 18 h prior to recording meaningful data. Experiments were performed in H_2SO_4 to ensure there were no copper-chloro complexes formed. Being able to ignore the effects of complexation allowed for the effects of free copper to be examined directly. Once the system was run in the absence of free chloride ions, the electrolyte was changed to 1 M HCl. This concentration was chosen in order to ensure the pH of the solution remained the same.

.

2.4 UV-Visible Spectroscopy

UV-visible spectroscopy (UV-Vis) experiments were performed on a Cary 60 UV- vis spectrophotometer. Solutions having various concentrations of $CuSO_4$ (0-40 ppm) were prepared in a 1 M HCl media. These solutions were placed into a quartz cuvette having a path length of 1 cm and placed into the instrument. The wavelength was scanned from 500-200 nm.

CHAPTER 3: HALF CELL EXPERIMENTS

3.1 Effect of pH in the Absence of Copper

Prior to investigating the effects of copper on this system, it was first necessary to perform baseline measurements in various concentrations of HCl in the absence copper. Solutions were prepared with concentrations of HCl ranging from 0.1 – 1.0 M. Results from cyclic voltammetry (CV) experiments can be seen in Figure 3.1. There is an increase in the peak current associated with hydrogen adsorption/desorption, which occurs in the low potential region. This is due to an increase in the proton concentration. There is also a notable increase in the peak current occurring near 1.2 V. This is due to the evolution of chlorine gas. This is evident as this potential corresponds to the standard reduction potential of chlorine, as shown in literature[35]

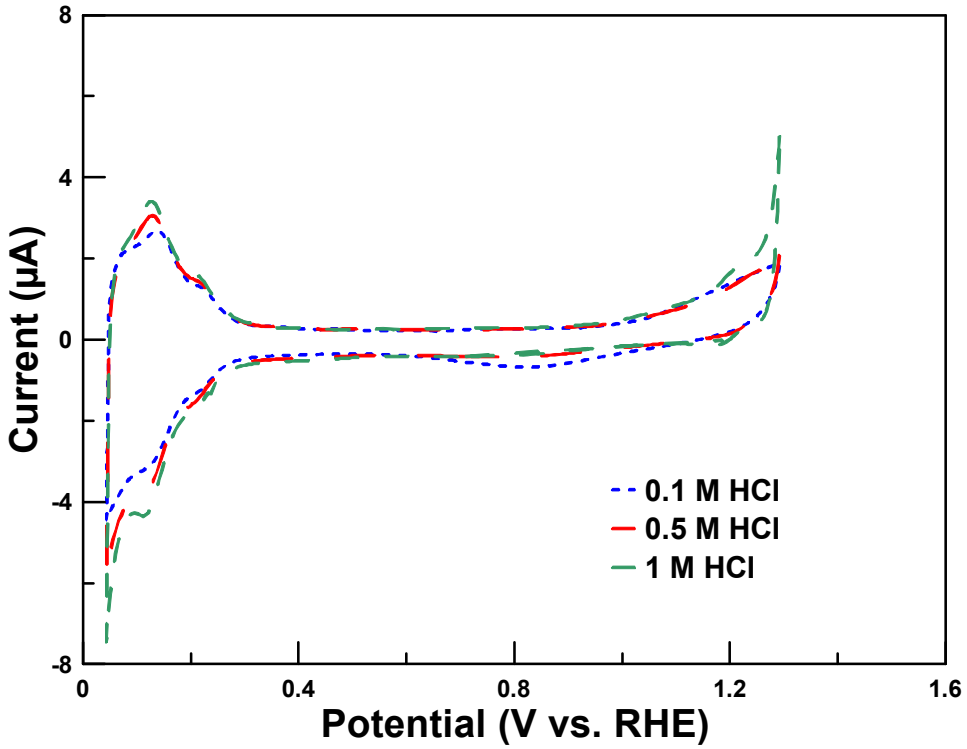

Figure 3.1: Cyclic voltammograms obtained for 0.1 M (blue), 0.5 M (red), and 1 M HCl (green), performed at a scan rate of 50 mV/s at 25 ℃ on 0.071 cm^2 planar Pt WE.

Figure 3.2 shows the variation of HER activity with increasing HCl concentration. As the concentration of HCl is increased, there is a dramatic increase in the current density for the HER. When the concentration was changed from 0.1 to 0.5 M, a large amount of noise begins to appear at more negative voltages due to bubble formation. There is also a notable decrease in the observed overpotential with increasing HCl concentration. This is due to the higher $[H^+]$ in the solution, minimizing the effects of migration of these ions to the electrode surface, lowering the energy required to begin the reaction.

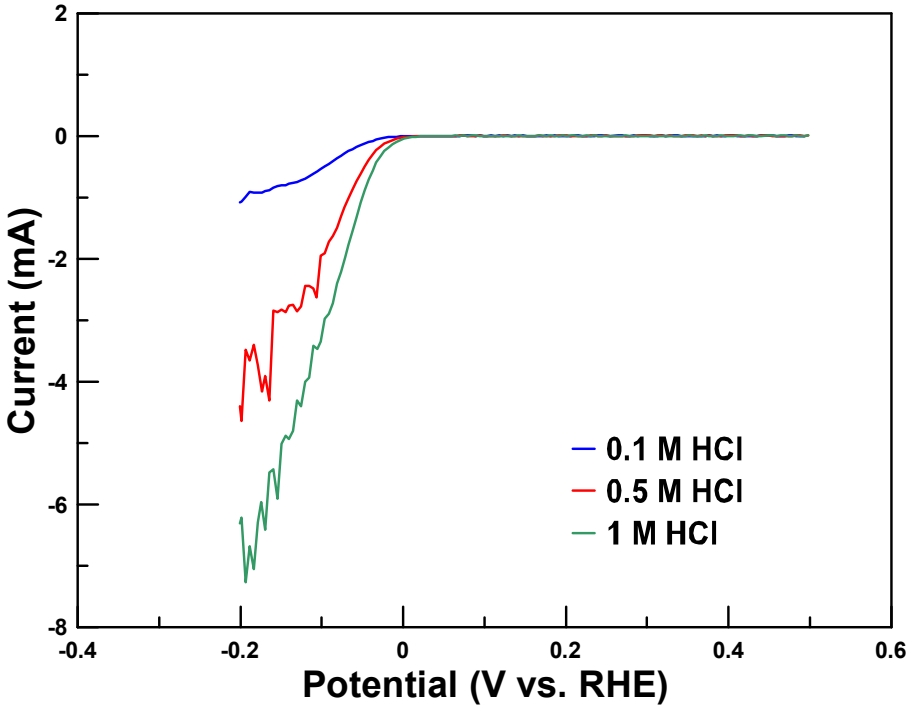

Figure 3.2: HER activity at a 0.071 cm^2 planar Pt WE of 0.1 M (blue), 0.5 M (red), and 1 M (green) HCl performed at a scan rate of 5 mV/s at 25 ℃

The same electrochemical system was examined using a Pt/C coated GC electrode. The results of the CV performed on each solution can be seen in Figure 3.3. These plots show a distinctly different trend than that of the 3 mm Pt working electrode. As the concentration of HCl increased, there was a distinct decrease in the peak current in the hydrogen adsorption and desorption region, indicating a decrease in the electrochemically active surface area (ECSA). This was a result of the increased concentration of Cl^- ions. Over the longer term, these chloride ions could promote the dissolution of Pt atoms through the formation of soluble Pt-Cl complexes, resulting in a decrease in ECSA[3536].

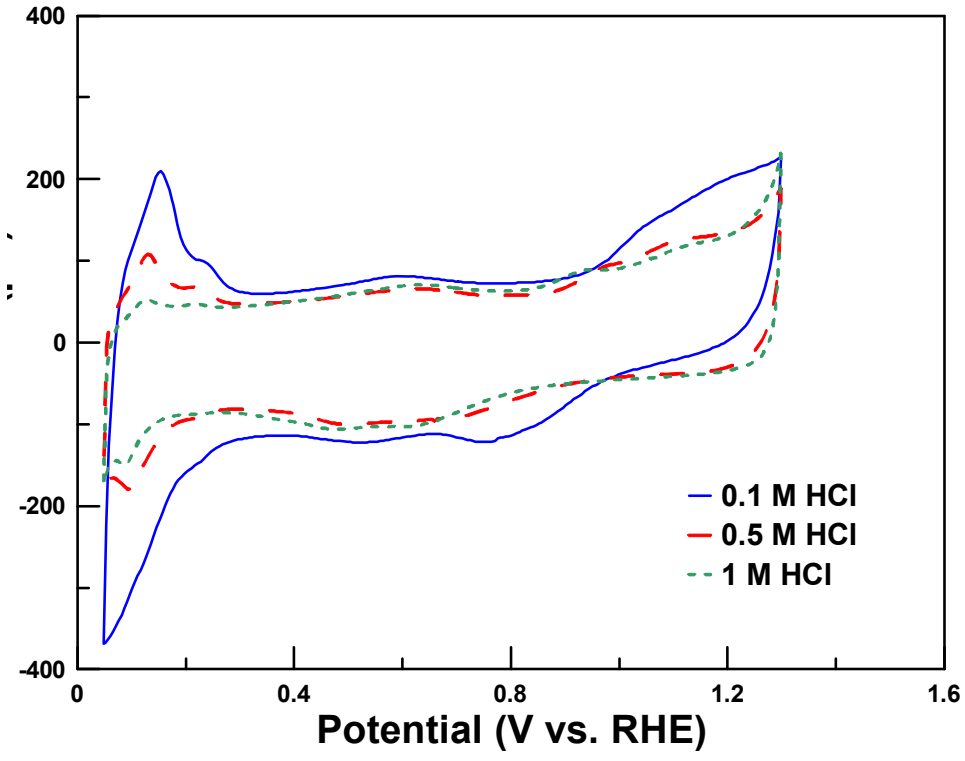

Figure 3.3: Cyclic voltammogram for 0.1 M (blue), 0.5 M (red), and 1 M (red) HCl on a 20% Pt/C on GC working electrode at 25 ℃ on 20% Pt/C-GC WE

The LSV results presented in Figure 3.4 show there was a dramatic increase in the current density proportional to the increase in the concentration of the HCl solution, which was also seen when using the pure Pt electrode. Increasing the HCl concentration results in an increase in the number of protons present. This reduces the effects of migration leading to increase HER kinetics. This is indicated by the increase in current density and decrease in overpotential

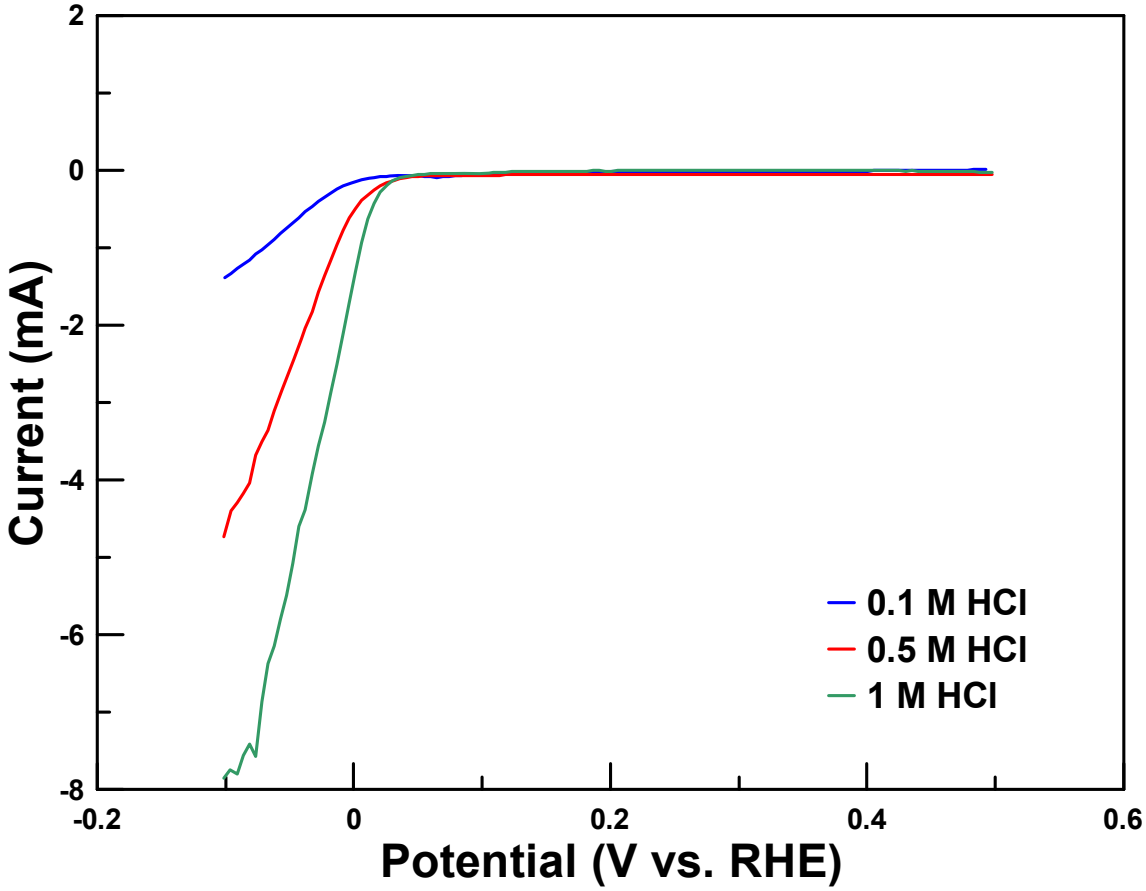

Figure 3.4: HER activity of 0.1 M (blue), 0.5 M (red) and 1 M (green) HCl on 20% Pt/C-GC WE at 25 ℃

3.2 Effect of Copper Concentration at Constant pH

Once a baseline was established by performing the desired electrochemical tests in the absence of copper contaminants, the next logical set of experiments to perform were ones in which both $[H^+]$ and $[Cl^-]$ were held constant, while varying the amount of Cu^{2+}. Results from cyclic voltammograms performed on these solutions can be seen in Figure 3.5. Near 0.75 V_{RHE}, a peak developed. This peak is the result of the Cu(II)/Cu(I) redox process, which became larger with increasing copper concentration. These tests show that Cu^{2+} is in fact detectable in this potential range. Upon examining the hydrogen adsorption/desorption region of these plots, it is clear that upon increasing the concentration of copper to 5 ppm there is no longer any definition of the different Pt facets. The peaks in this region have little definition, making it difficult to distinguish individual peaks arising from specific facets of Pt. This is due to the plating of copper onto the polycrystalline Pt surface, which hinders the adsorption of protons onto the Pt surface and effectively reducing the ECSA[33]. There is no significant change in the size of the peak at the opposite end of the voltage window because there was no change in the chloride concentration. This means that the amount of chloride evolved at this potential should remain the same.

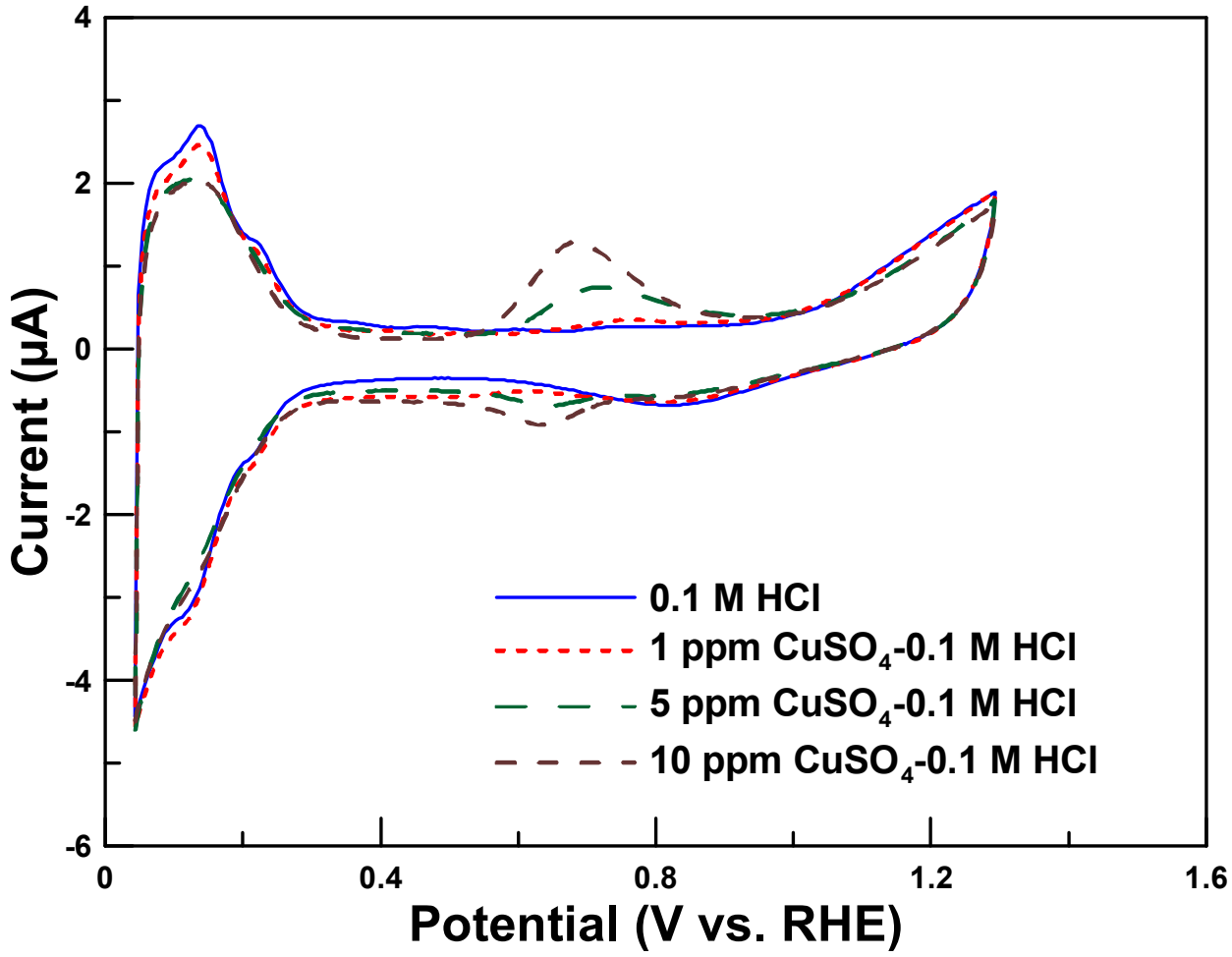

Figure 3.5: Cyclic voltammogram for solutions of 0.1 M HCl (blue), 1 ppm (red), 5 ppm (green), and 10 ppm (brown) $CuSO_4$ at a 0.071 mm^2 Pt WE performed at a scan rate of 50 mV/s at 25 ℃

LSV tests performed at various copper concentrations can be seen in Figure 3.6. As the concentration of copper was increased there appeared to be a significant increase in overpotential and decrease in current density. This indicates that copper is in fact blocking Pt active sites effectively poisoning the electrode surface.

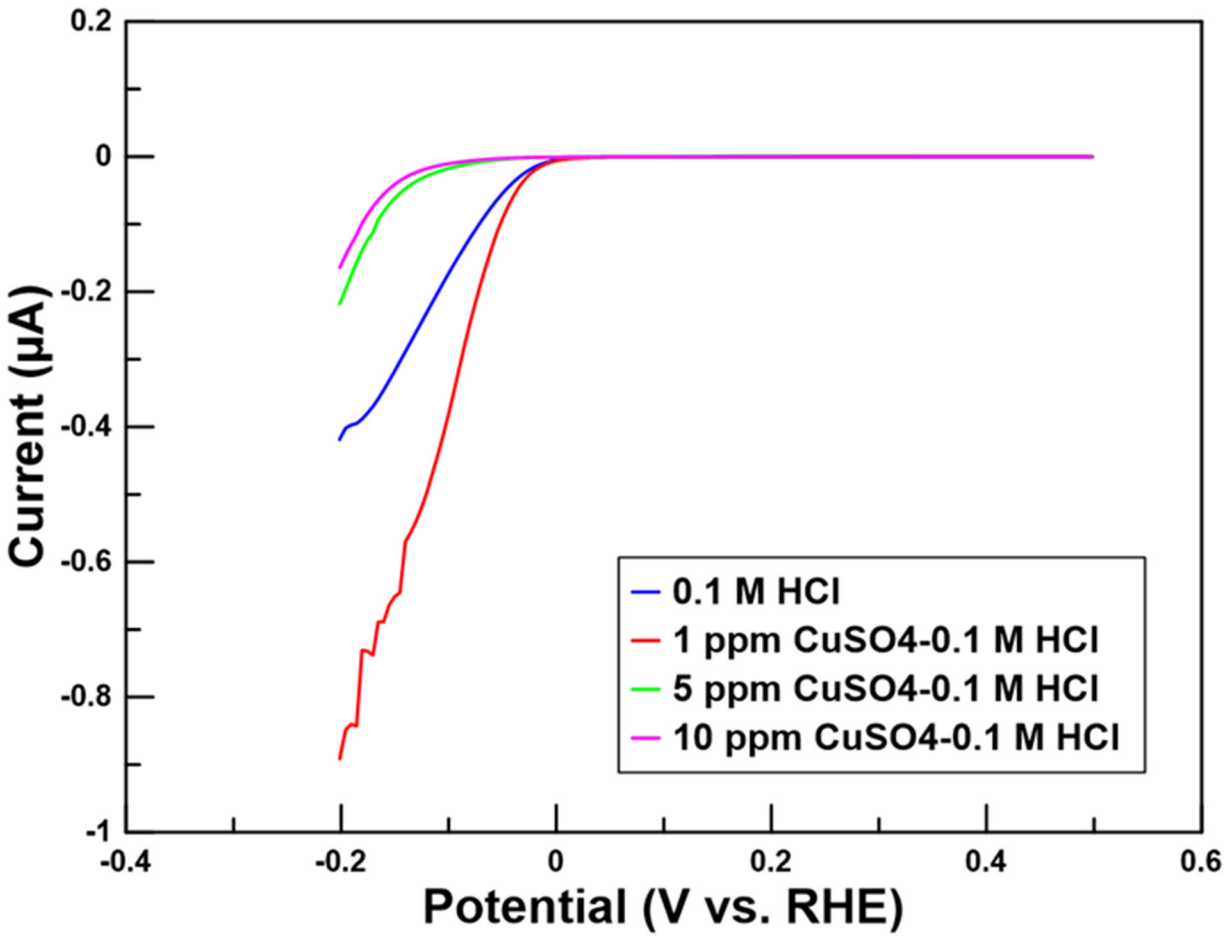

Figure 3.6: HER activity of 0.1 M HCl and 0 ppm (blue), 1 ppm (red), 5 ppm (green), and 10 ppm (purple) $CuSO_4$ on 0.071 cm^2 Pt WE performed at a scan rate of 50 mV/s at 25 ℃

The same tests were repeated using the 20% Pt/C on GC working electrode. CV results can be seen in Figure 3.7. These show that there is no significant difference in the peak current in the hydrogen adsorption/desorption region when the concentration of copper was raised to 1 ppm. Once the concentration was increased to 5 ppm however, there appears to be an increase in the peak current in this region. This can be attributed to an effect known as copper underpotential deposition. This is a phenomenon in which a monolayer is formed on the surface of a metal

substrate at a potential positive of the Nernst potential [37]. Once the concentration is increased to 10 ppm this effect is no longer observed. This is due to the fact that the effects of copper plating have surpassed those of copper UPD. Another feature of the plots presented in Figure 3.7 that should be noted is the absence of the peak occurring near 0.7 V_{RHE} that was present in the results obtained using the planar Pt electrode. This is a result of the increased surface area coupled with the low copper concentrations employed in this study. Additionally, carbon is increasing the capacitive background current making the Cu peaks difficult to distinguish. Since there is a dramatic increase in the number of Pt active sites the effects of copper are no longer above the limit of detection for this system. LSV experiments show a notable dip in the current density just before the 0 V mark. This is due to the adsorption of hydrogen into the film, minimizing the extent of the effects of migration and allow for H-UPD. The onset potential does shift to slightly more negative potentials in the upon increase of the copper concentration. This could potentially be due to some of the current is going into Cu UPD. There appears to be no impact on the current density due to the effects of Cu^{2+}. LSV results obtained for these experiments can be seen in Figure 3.8.

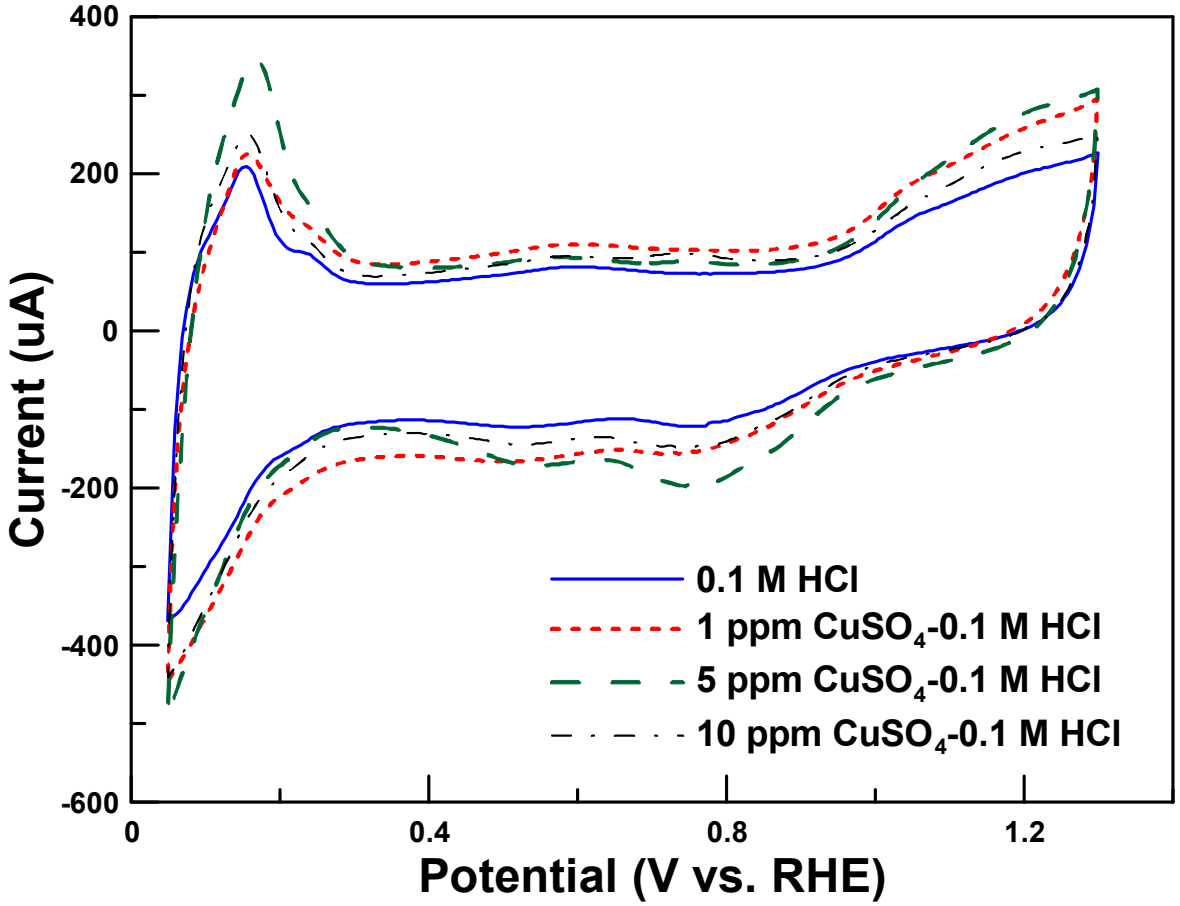

Figure 3.7: Cyclic voltammogram for solutions of 0.1 M HCl and 0 ppm (blue), 1 ppm (red), 5 ppm (green), and 10 ppm (black) $CuSO_4$ at a 20% Pt/C-GC WE performed at a scan rate of 50 mV/s at 25 ℃

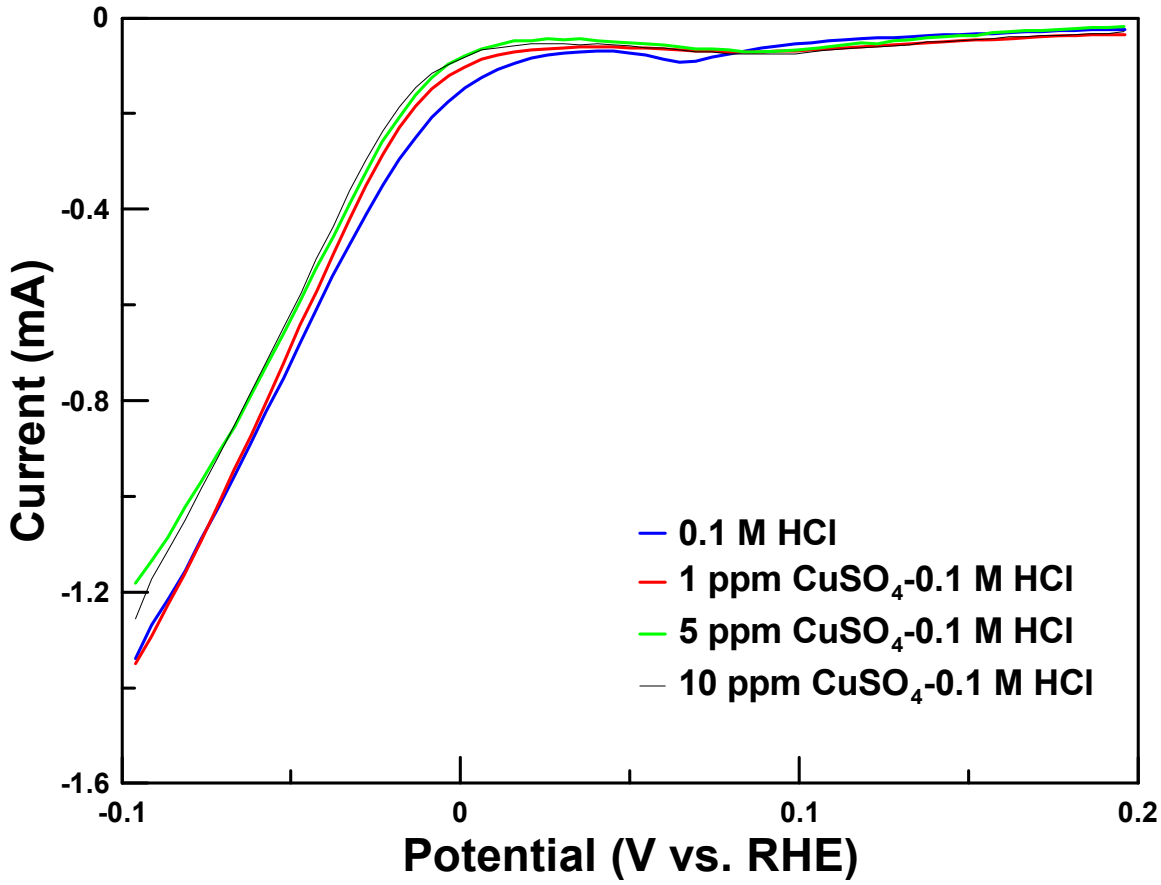

Figure 3.8: HER activity of 0.1 M HCl and 0 ppm (blue), 1 ppm (red), 5 ppm (green), and 10 ppm (black) $CuSO_4$ at a 20% Pt/C-GC WE at a scan rate of 5 mV/s at 25 ℃

3.3 Variable [Cu^{2+}] in Chloride Free Medium

To fully understand the importance of the role of free chloride ions on Pt surface health, as well as the efficiency of the HER, it was necessary to perform electrochemical tests in a chloride free media. This was achieved by employing $HClO_4$ in place of HCl. The concentration was held at 0.1 M in order to ensure that the pH of the solution remained the same as those experiments performed in a solution of 0.1 M HCl. The concentration of $CuSO_4$ was increased from 0-10 ppm

as in previous experiments. There is a distinct anodic peak that begins to show up near 0.75 V_{RHE} when the $CuSO_4$ concentration reaches 1 ppm. This peak gets larger as the concentration of Cu^{2+} increases. These results show that the presence of copper is detectable when there is no chloride present in the supporting solution. CV results obtained from these experiments can be seen in Figure 3.9

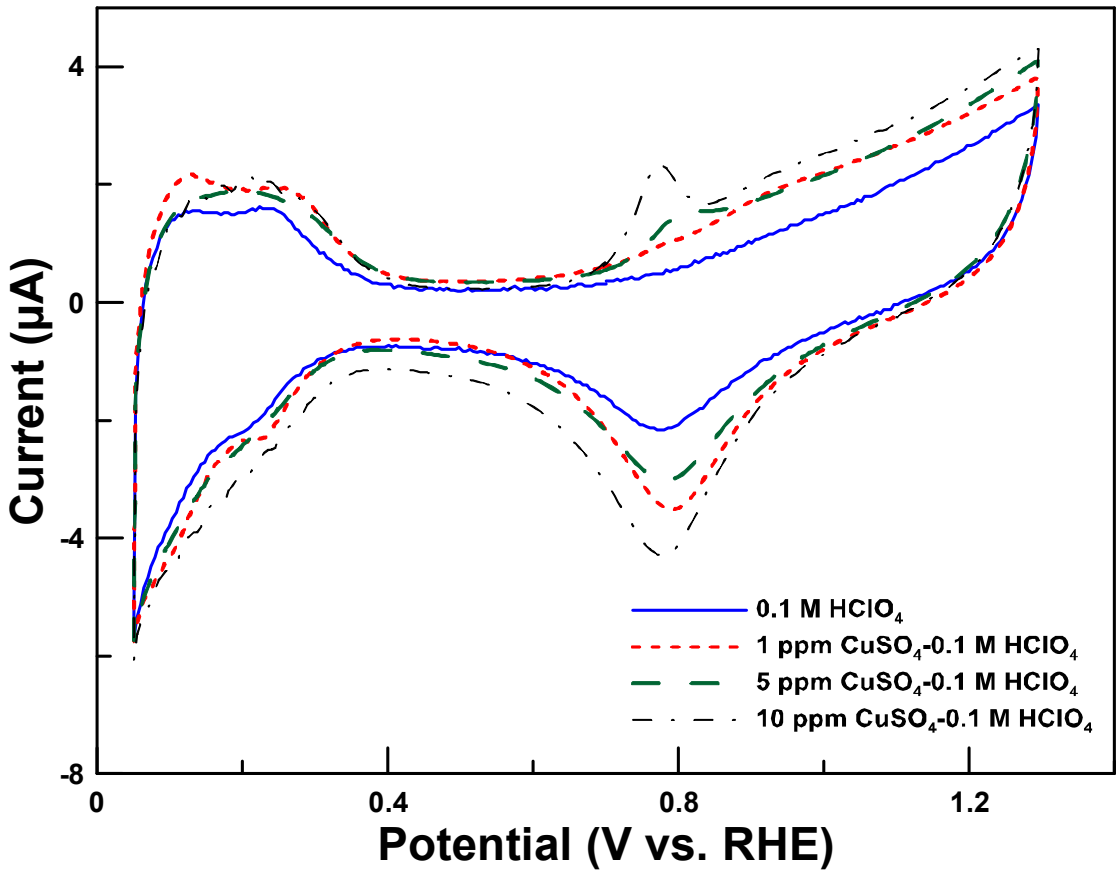

Figure 3.9: Cyclic voltammograms performed in 0.1 M $HClO_4$ with 0 ppm (blue), 1 ppm (red), 5 ppm (green), and 10 ppm (black) $CuSO_4$ performed at a scan rate of 50 mV/s on 0.071 cm^2 planar Pt WE at 25 ℃

LSV tests were performed with for all of the same copper concentrations in $HClO_4$ and are shown in Figure 3.10. Results show that there is a large increase in the overpotential required for the HER. There is a notable trend in the observed current density and in turn the reaction efficiency. As the concentration of Cu^{2+} is increased, the current density decreases dramatically. This could be due to the fact that all Cu^{2+} ions are free in solution, as there are no free chloride ions availble for complexation. This would increase the number of Cu ions near the electrode surface which are able to bond to the Pt active sites located on the negatively charged electrode.

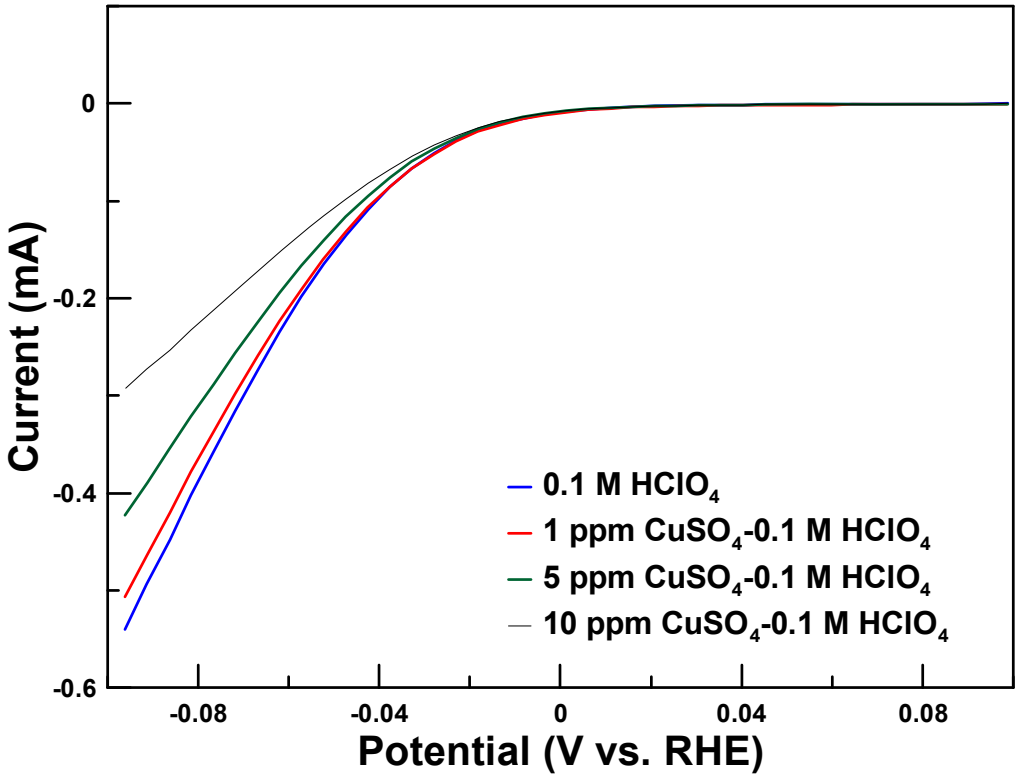

Figure 3.10: HER activity in 0.1 M $HClO_4$ with 0 ppm Cu^{2+} (blue, 1 ppm Cu^{2+} (red), 5 ppm Cu^{2+} (green), and 10 ppm Cu^{2+} (purple) performed at a scan rate of 50 mV/s on 0.071 cm^2 Pt WE at 25 °C

3.5 Summary

In this section the effects of copper were investigated by employing a three-electrode cell configuration. The Pt surface health was examined by running the system at positive potentials and the HER activity investigated by running the system in the negative potential regime. These tests were employed to provide insight into how the system would perform in the full cell configuration. Two different working electrodes were used; a 0.071 cm^2 Pt planar electrode and a 0.071 cm^2 GC electrode coated with 20% Pt/C ink.

Tests were performed in the absence of copper contaminant to develop a baseline. During these experiments, the concentration of HCl was varied from 0.1-1 M. The peaks present in the hydrogen adsorption/desorption region increased slightly with increasing HCl concentration. HER activity was also shown to increase. Results from CV experiments performed using a 20% Pt/C coated GC electrode show a decrease in the peak current in the hydrogen adsorption/desorption region blockage by adsorbed Cu species, resulting in a decrease in ECSA.

Solutions were prepared with a constant HCl concentration of 0.1 M while the Cu^{2+} concentration was varied from 0-10 ppm. CV results showed a peak that begins to resolve near 0.75 V_{RHE} as the Cu^{2+} concentration was increased. This peak becomes visible when the $[Cu^{2+}] \geq$ 5 ppm. HER activity for these experiments showed that there is a significant decrease in current density and increase in overpotential at the same concentration threshold. This indicates that the presence of copper ions in solution does in fact negatively impact HER kinetics. The same experiments were performed using a 20% Pt/C coated GC electrode. CV results from these tests do not exhibit the peak observed near 0.75 V_{RHE} as there is a significant increase in the surface area, causing the small amount of copper present in solution to fall below the limit of detection.

The HER kinetics also appear to be unaffected by the presence of trace amounts of copper at such high surface areas.

Tests were performed in $HClO_4$ in order to determine the effects of copper in the absence of chloride ions. CV results show the development of a peak at 0.8 V_{RHE} that increases with increasing Cu^{2+} concentration. This peak is not visible until the concentration of copper was raised to 5 ppm. HER activity showed a decreased efficiency with increasing [Cu^{2+}] indicated.

CHAPTER 4: FULL CELL EXPERIMENTS

** Parts of the work described in this chapter has been published as:

S.L. Cobourn, E.B. Easton, “The effect of copper contamination at the cathode of CuCl/HCl electrolyzers", *International Journal of Hydrogen Energy, 42 (*2017) 28157 - 28163. doi:10.1016/j.ijhydene.2017.09.142

4.1 Conventional Water Electrolysis

To ensure the electrolysis system constructed in house was operating properly, conventional water electrolysis tests were performed with the potential being scanned from 1.0 – 2.0 V. These tests allowed us to determine the effectiveness of the MEA preparation as well as the system set up. Linear sweep voltammetry was performed in a positive direction as conventional water electrolysis occurs at a potential of approximately 1.2 V according to the literature. As expected, at this potential the current density began to increase. However, there is not a significant increase in the current until about 1.8 V was applied to the system. This is typically seen in practical cells as there is a significant overpotential and large Ohmic drop associated with this reaction [22]. This shows that the system does in fact, function successfully as a water electrolysis cell. The LSV plot obtained during this particular test configuration can be seen in Figure 4.1.

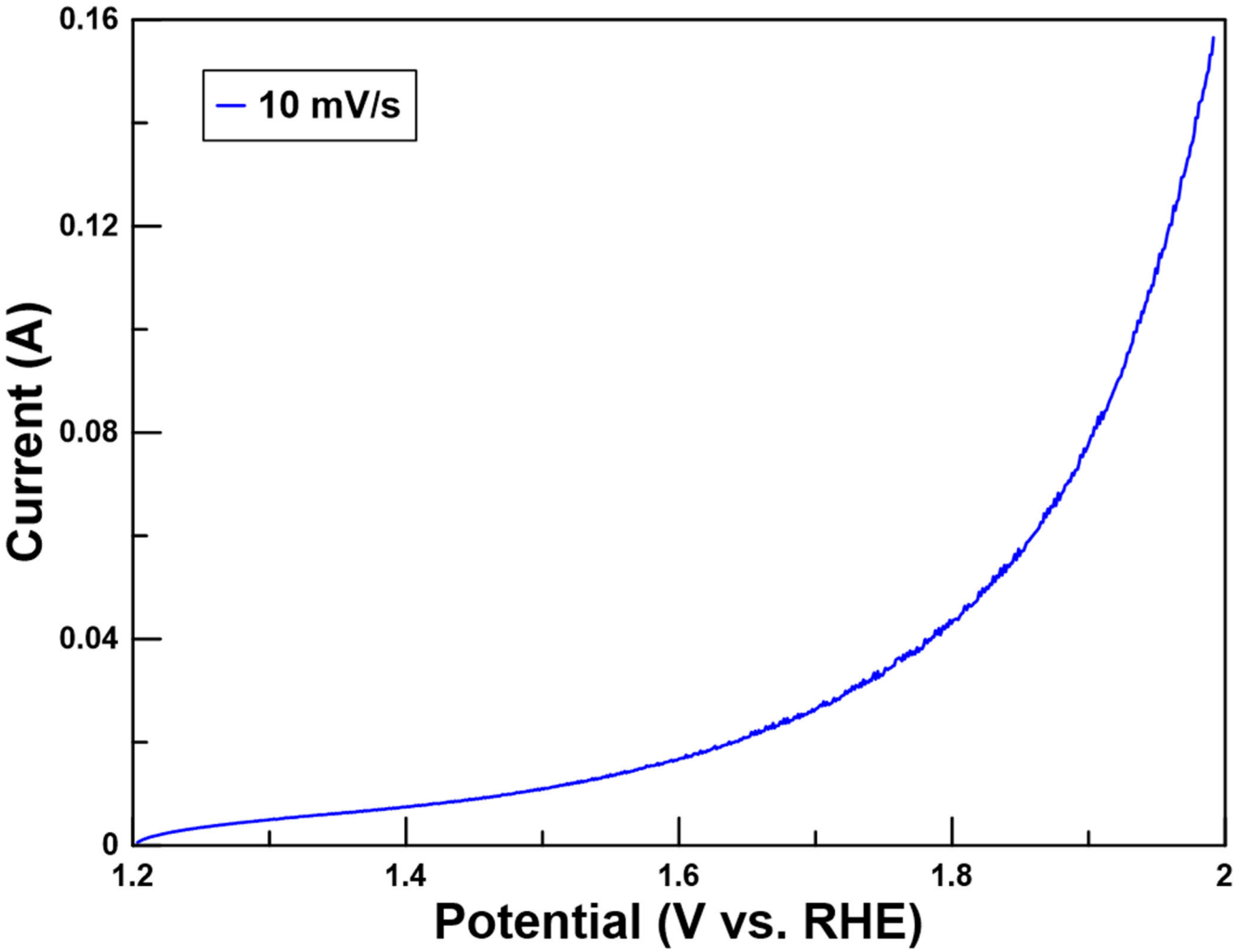

Figure 4.1: HER activity for conventional water electrolysis performed at a scan rate of 10 mV/s in full cell configuration at 25 ℃

4.2 Measurements using 0.5 M H_2SO_4

Following the system validation described in the previous section, the system was run in proton pump mode in the absence of chloride. These tests were essential for determining the true effects of trace copper contamination at the cathode as they allowed for complete control over the concentration of copper at the cathode. Using this approach provides insight into the actual amount

of trace Cu^{2+} that this electrochemical system is able to maintain voltage and/or Coulombic efficiency as it pertains to hydrogen production. The concentration of copper sulfate was varied between 0-10 ppm.

Cyclic voltammograms were performed in order to investigate the Pt surface health. The plots for these experiments can be seen in Figure 4.2. In the absence of copper there appears to be a small peak present in the CVs that occurs near 0.7 V vs RHE. This can be attributed to the oxidation of quinone groups on the carbon electrode surface. In the absence of copper, we see the typical peak in the hydrogen adsorption/desorption region of the voltammogram. As the concentration of copper is increased, there is an increase in the peak current observed in this region. This is most likely due to copper underpotential deposition (UPD). Copper UPD is a phenomenon that that occurs when the reaction conditions allow for the reduction of Cu at potentials that are positive of the standard reduction potential [38]. This shows that the presence of copper does in fact have an effect on the Pt surface atoms at concentrations as low as 1 ppm. When the concentration of $CuSO_4$ is raised to 10 ppm however, we see a depression in the peak current in the hydrogen adsorption/desorption region compared to that of the 0 ppm Cu^{2+} solution. This is due to copper plating, which blocks the Pt active sites.

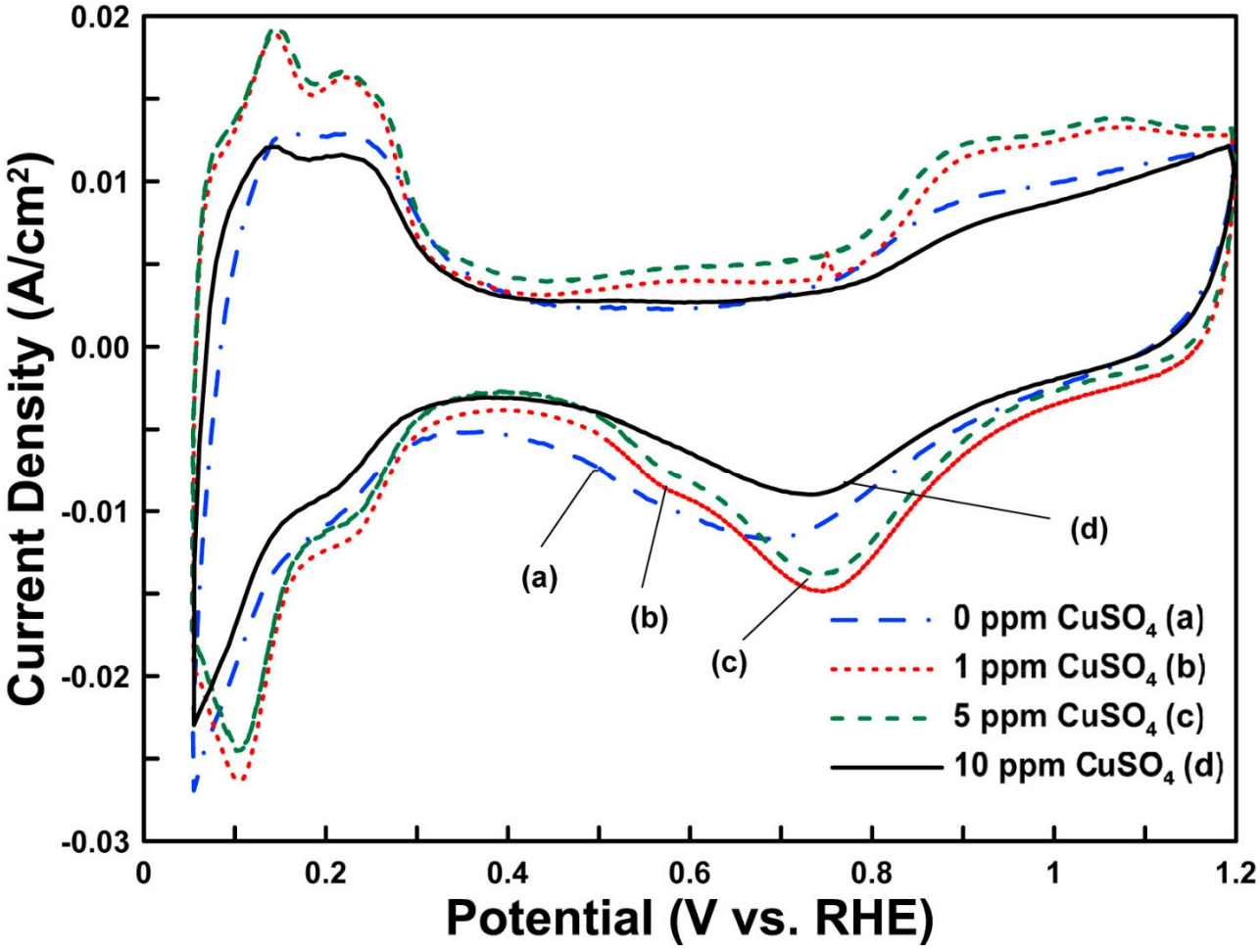

Figure 4.2: Cyclic voltammograms performed in 0.5 M H_2SO_4 contaminated with 0 ppm (blue), 1 ppm (red), 5 ppm (green) and 10 ppm $CuSO_4$ at a scan rate of 50 mV/s in full electrolysis cell run in "proton-pump" mode at 25 ℃

Linear sweep voltammetry experiments were performed in order to provide insight into the effect of copper concentration on the overpotential and efficiency of the HER at the Pt/C electrode in the absence of free chloride ions. These voltammograms were obtained by scanning from positive to negative potentials. In the absence of copper, there appears to be little to no over potential associated with the HER. There is also a relatively large current density associated with this reaction. There is no free copper present in the solution and therefore, no possibility of copper plating effecting the cell performance.

When the concentration of $CuSO_4$ is increased to 1 ppm, there is a 9% decrease in the observed current density at -0.2 V, a trend which continues as the concentration of copper is further increased to 5 ppm. Upon raising the concentration of copper to 10 ppm, however, there is a dramatic decrease in the resulting current density, showing a 48% decrease relative to the current density obtained in the absence of copper contaminant. There is a notable increase in the onset potential for the HER. These results suggest that copper is having a significant effect on the hydrogen evolution reaction kinetics. Data obtained from these experiments can be seen in Figure 4.3.

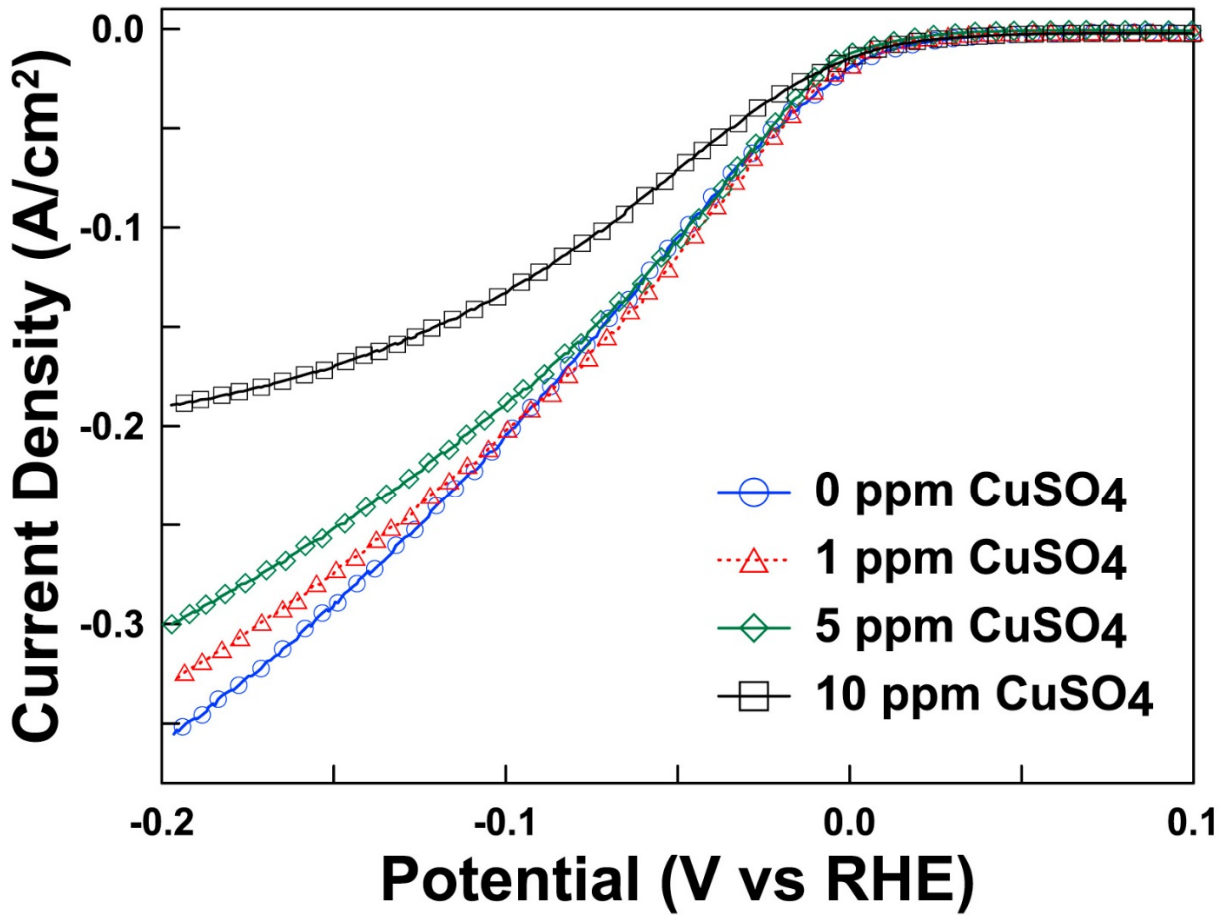

Figure 4.3: Linear sweep voltammograms in 0.5 M H_2SO_4 running system in proton pump mode at various [Cu^{2+}] performed at a scan rate of 5 mV/s at 25 ℃

If the presence of Cu leads to a significant amount of current going into Cu plating instead of HER, there should be a change in the amount of hydrogen gas produced. To investigate this, galvanostatic hydrogen production was performed with varying concentrations of copper added to the catholyte solution. Again, the resulting potential should reflect the overpotential required to perform the HER at a constant current density. The variation in cell potential at various copper concentrations as well as the overpotential as a function of copper concentration can be seen in

Figure 4.4. It is evident that at all copper concentrations the potential shows a large initial dip, which is due to the stabilization of the system at the employed current density. After this point there is little to no change in the observed potential for the duration of the experiment. As the concentration of copper is increased, there is a notable decrease in the negative potential required to maintain the current density chosen. This increased overpotential arises from the need to first remove adsorbed Cu species from the Pt surface before HER can proceed..

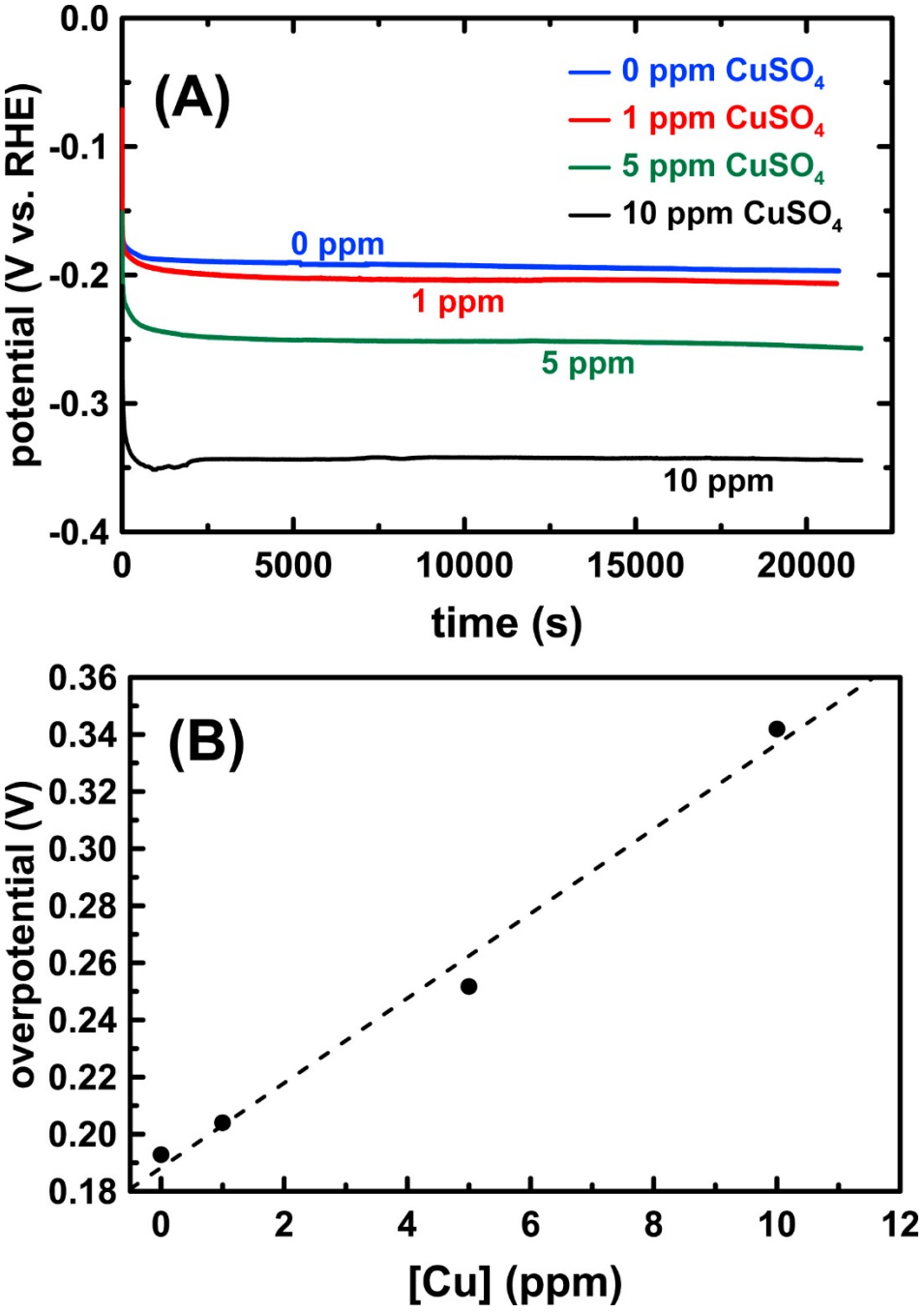

Figure 4.4: A) Galvanostatic curves at 1.5 amps and 25 ℃ obtained during hydrogen production experiments performed in proton pump mode at various [Cu^{2+}] concentrations and B) Overpotential as a function of copper concentration as obtained from data in Figure 4.4-A.

It was possible to determine the amount of hydrogen gas produced at the cathode by following the mass of water displaced and further converting that mass to moles of hydrogen gas. The moles of hydrogen gas was then plotted against the time elapsed. This particular set of experiments are galvanostatic, therefore there should be a linear relationship between the time elapsed and the number of moles of hydrogen produced. If in fact there was an effect on the Coulombic efficiency of the reaction, there would be a change in the rate of hydrogen production. This does not appear to be the case as the relationship is nearly perfectly linear. All of the copper concentrations tested in this set of experiments give the same response. Furthermore, rate of hydrogen production does not change with increasing copper concentration. The hydrogen production efficiency determined also appeared to be unaffected by the amount of copper present in solutions, which should be expected based on the consistency of the hydrogen production rate at all copper concentrations. Figure 4.5(A) shows the moles of hydrogen produced as a function of time for various copper concentrations and the respective hydrogen production efficiencies. Results from these experiments indicate that there is no effect on the Coloumbic efficiency due to the presence of Cu^{2+}, however there does appear to be a significant effect on the voltage efficiency. This suggests that copper is adsorbed to the surface and there is no electron transfer taking place. The threshold for copper tolerance before the voltage efficiency is significantly affected appears to be 5 ppm.

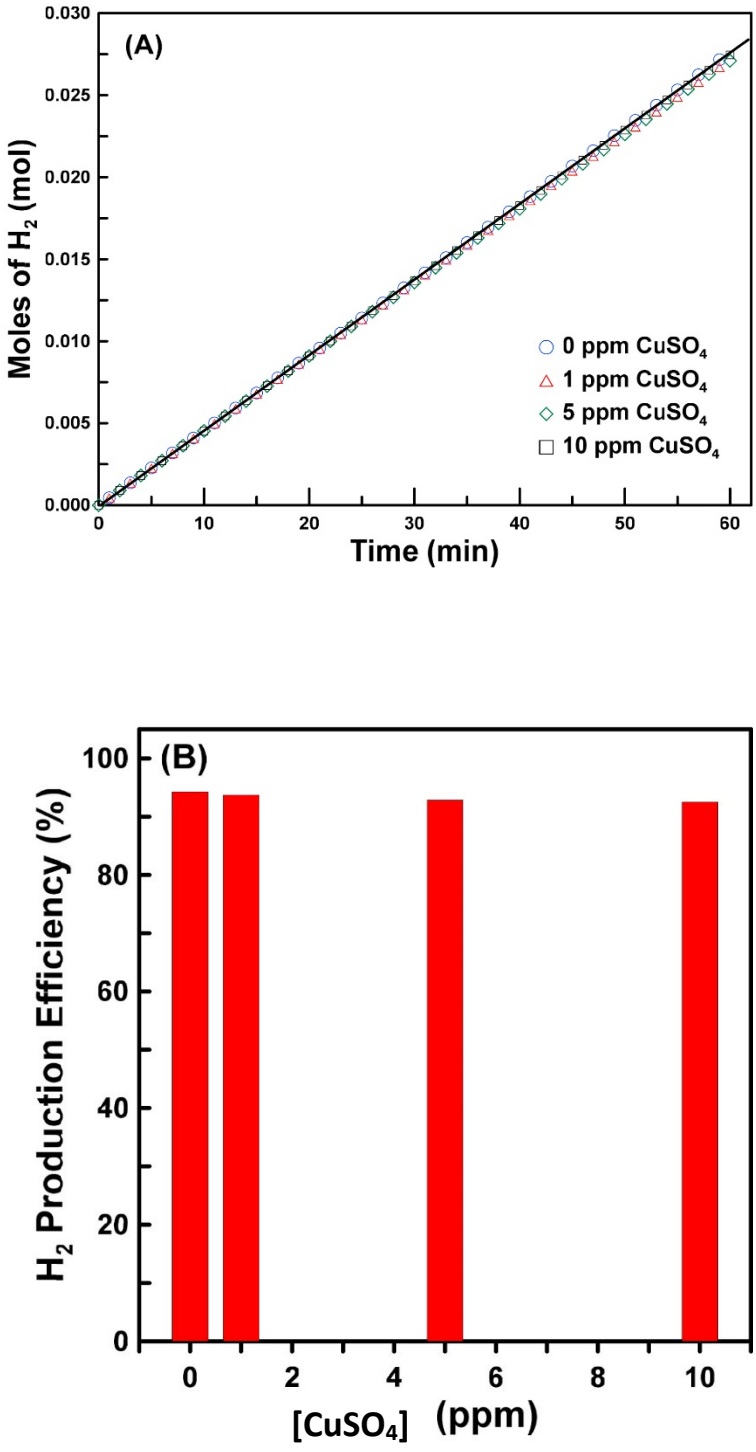

Figure 4.5: A) Moles of H_2 produced as a function of time and B) Hydrogen production efficiency for various copper concentrations at 25 ℃ performed in full cell in "proton-pump mode" at a constant current density 300 mA/cm^2

4.3 Contaminated 1 M HCl

The same electrochemical tests were performed in 1 M HCl as were performed in 0.5 M H_2SO_4. The concentration of HCl employed was 1 M in order to ensure the pH remained the same between the two data sets. Due to the fact that there are free chloride ions present in the solutions tested in this set of experiments, there will of course be some copper-chloro species formed, thereby limiting the amount of copper available to plate onto the electrode. There are five different possible complexes that could potentially form. Which complexes are present depends on the concentration of chloride atoms as well as the concentration of copper. It is possible to follow the formation of the various copper-chloro complexes as a function of either parameter using UV-visible spectroscopy (UV-Vis). This was shown in the work performed by Uchikoshi et al., who studied the different complexes that were formed using Cu^{2+} as a function of the concentration of the HCl electrolyte. This held the concentration of Cu^{2+} constant at 27 ppm, while the HCl concentration was varied between 0.002-5.57 M. The observed peaks corresponded to the increase/decrease of particular copper-chloro species. The peak position and corresponding complex formula can be found in Table 4.2. As a control, we reproduced those experiments, and the UV-vis spectra are shown in in Figure 4.6. These results match those obtained by Uchikoshi et al. and therefore this technique can be considered valid for examining the speciation of these complexes in our particular system.

Table 4.1: Position of peak in UV-vis spectrum for various copper-chloro complexes at 298 K[39]

Cu-Cl Complex	Peak Position (nm)
Cu^{2+}	230
$CuCl^{+}$	250
$CuCl_2^{0}$	275
$CuCl_3^{-}$	385
$CuCl_4^{2-}$	375

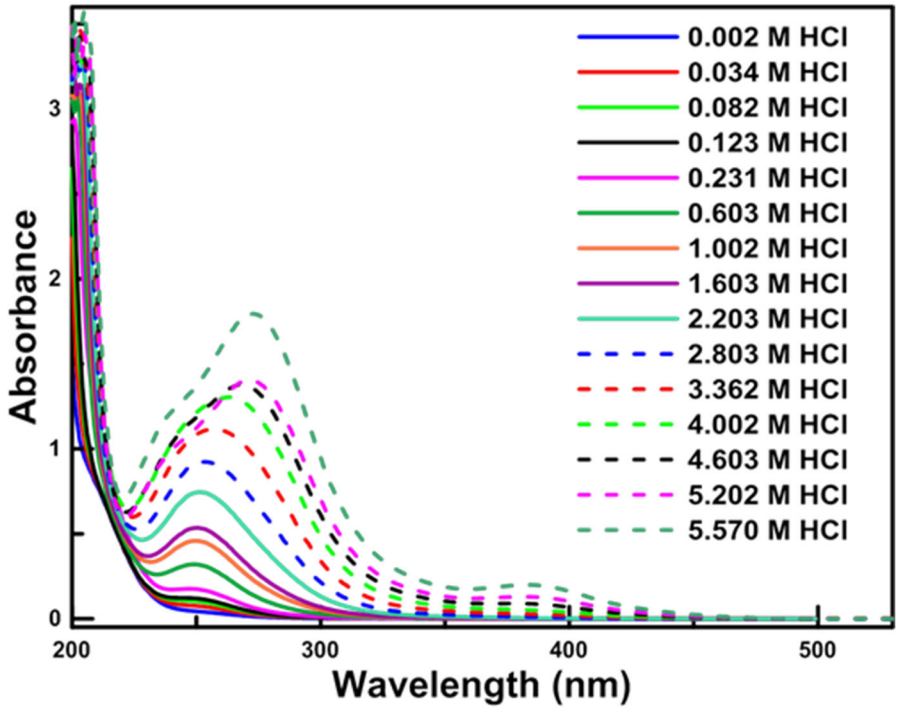

Figure 4.6: Calibration curve for copper speciation at 27 ppm $CuSO_4$ various HCl concentration determined by UV-visible spectroscopy

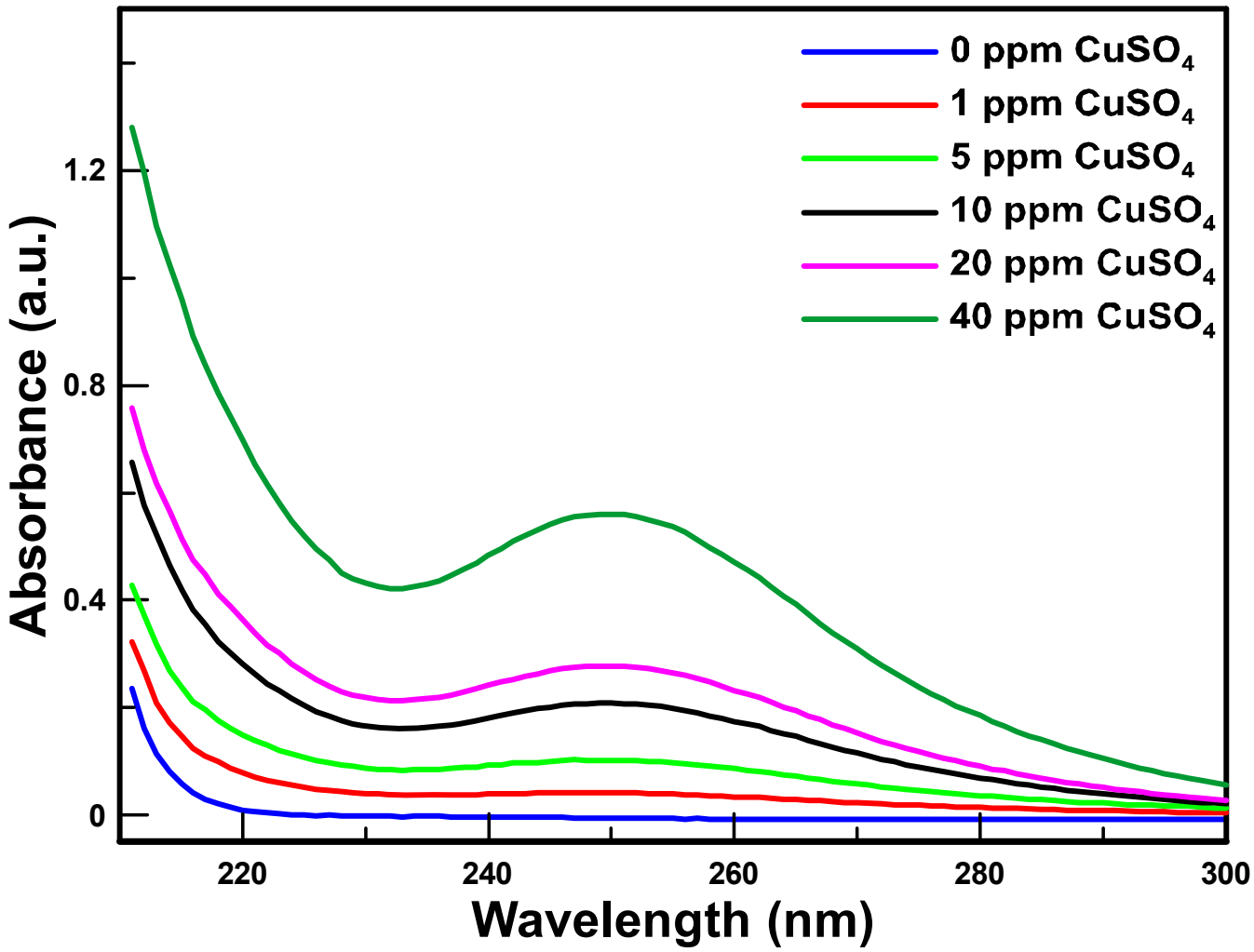

Figure 4.7: UV-Vis spectra obtained at various $CuSO_4$ concentration in 1 M HCl at ambient temperature and pressure

Since the concentration of HCl is held constant during these experiments, only the amount of copper present in solution is relevant. The point at which any peaks are observed in the range explored will give direct information as to the exact species present at that concentration of copper. The UV-vis spectra obtained at different concentrations of Cu^{2+} in 1 M HCl can be seen in Figure 4.7. In the absence of copper contaminant there is no notable peaks that can be detected by this

instrument which is of course expected as the scanning window was chosen to only incorporate the expected copper-chloro complexes that could potentially form. When the concentration of copper was increased a peak appears near 250 nm and grows proportionally to the amount of copper present in solution. This peak corresponds to the $CuCl^+$ complex as found in literature [39]. Since the concentration of copper tested in this set of experiments greatly surpasses the concentrations employed during the electrochemical tests performed, it can be confidently stated that the only complex that should be expected to form in the solutions should be in the form of $CuCl^+$. Due to the fact that the complexes formed at this HCl concentration, the positive charge associated with this species would still allow for crossing of the cationic exchange membrane.

Results from CV experiments performed at varying $CuSO_4$ concentrations can be seen in Figure 4.8. These tests were again performed in order to Once again we see a small peak occurring at approximately 0.6 V, which can be attributed to the presence of quinone groups on the carbon electrode material. Once the concentration of copper in solution is raised to 10 ppm there is a clear depression in the peak current in this area. It is also worth noting that the peaks that typically represent each of the three platinum facets have now lost their definition, giving the peak a more smoothed/broadened appearance. This particular set of results show that when the concentration of the copper was raised to this level there is indeed a negative impact on the Pt surface health.

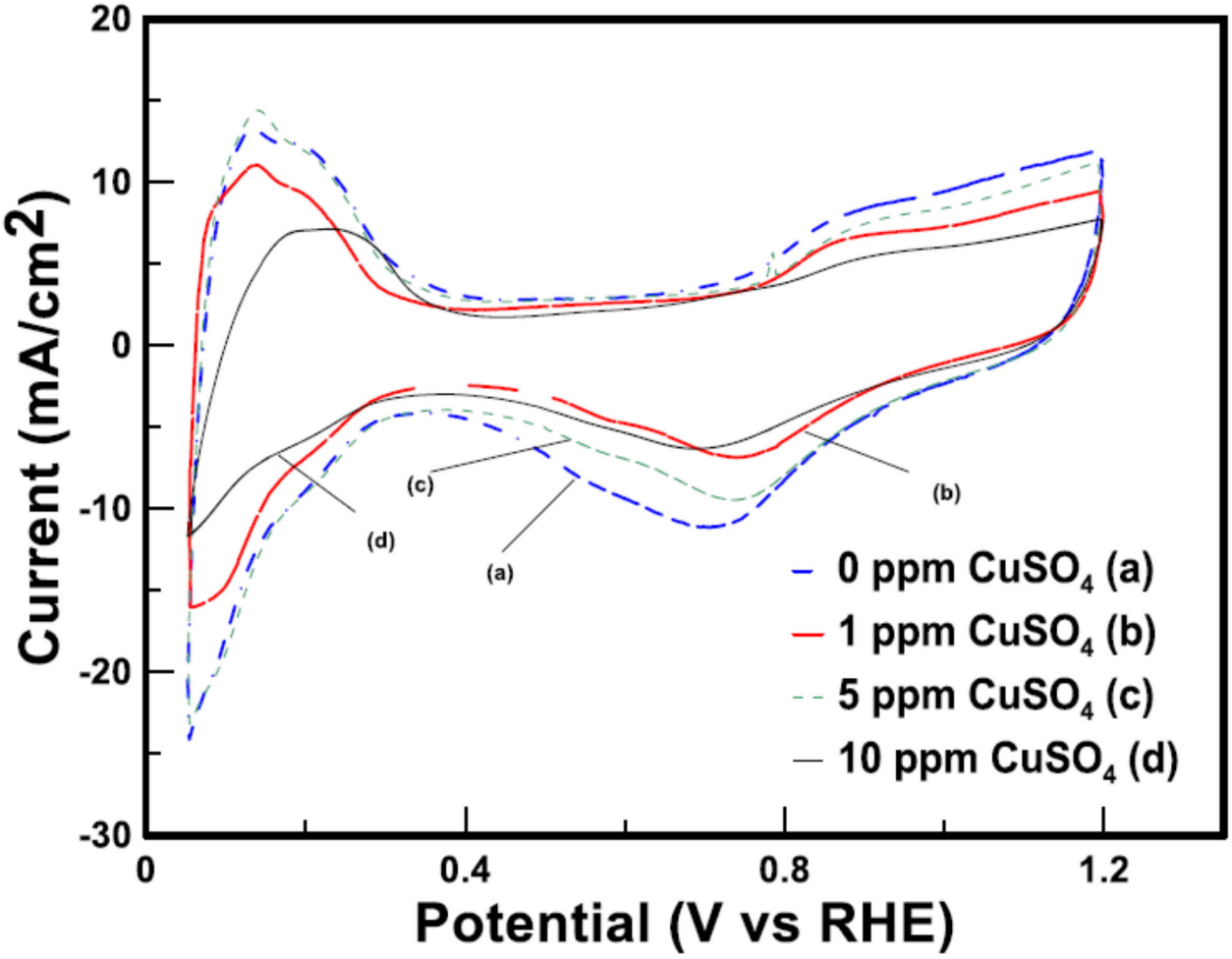

Figure 4.8: Cyclic voltammograms performed in 1 M HCl with various copper concentrations performed at a scan rate of 50 mV/s at 25 ℃

LSV results obtained in HCl can be seen in Figure 4.9. HER activity closely resembles those observed in H_2SO_4, with there being only a slight increase in the overpotential or and decrease in current density upon increasing the concentration of the $CuSO_4$ from 0 to 5 ppm. Once the concentration was raised to 10 ppm there was a dramatic decrease in the observed current density. There was also a significantly negative effect on the onset potential. These

results show that Cu has an effect on HER kinetics when the concentration is raised above 5 ppm.

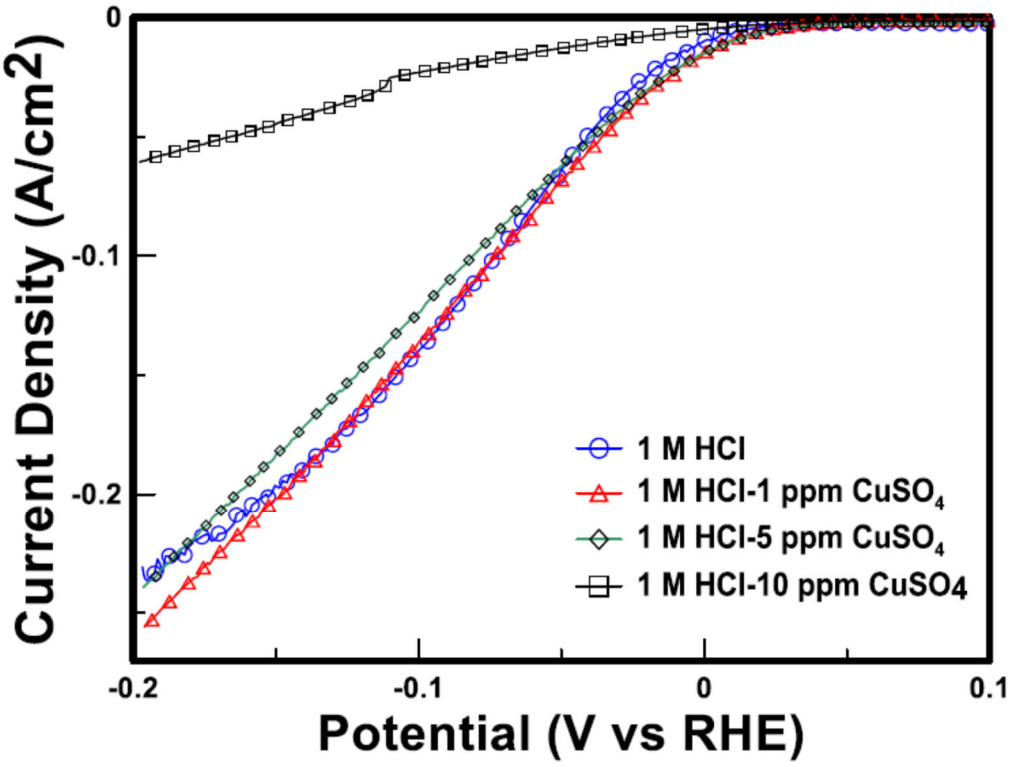

Figure 4.9: HER activity in 1 M HCl running system in proton pump mode with various [Cu^{2+}] performed at a scan rate of 5 mV/s at 25 ℃

Results from galvanostatic experiments performed with these solutions are shown in Figure 4.10. There is a significant increase in the potential associated with the HER proportional to the increase in copper concentration. This shows that the presence of copper has a negative

effect on the voltage efficiency of the HER. The amount of hydrogen gas produced at the cathode was monitored and it was determined that the hydrogen production efficiency remained unaffected by the presence of copper contaminant. The hydrogen production efficiency calculated at each copper concentration is shown in Figure 4.11(B). The number of moles of hydrogen produced over time was plotted and the results can be found in Figure 4.11(A). There is clearly a linear relationship between the time elapsed and the number of moles produced. The fact that there is no change in the slope as the amount of time elapsed indicates that the rate of hydrogen production remains constant, regardless of the amount of copper present in solution.

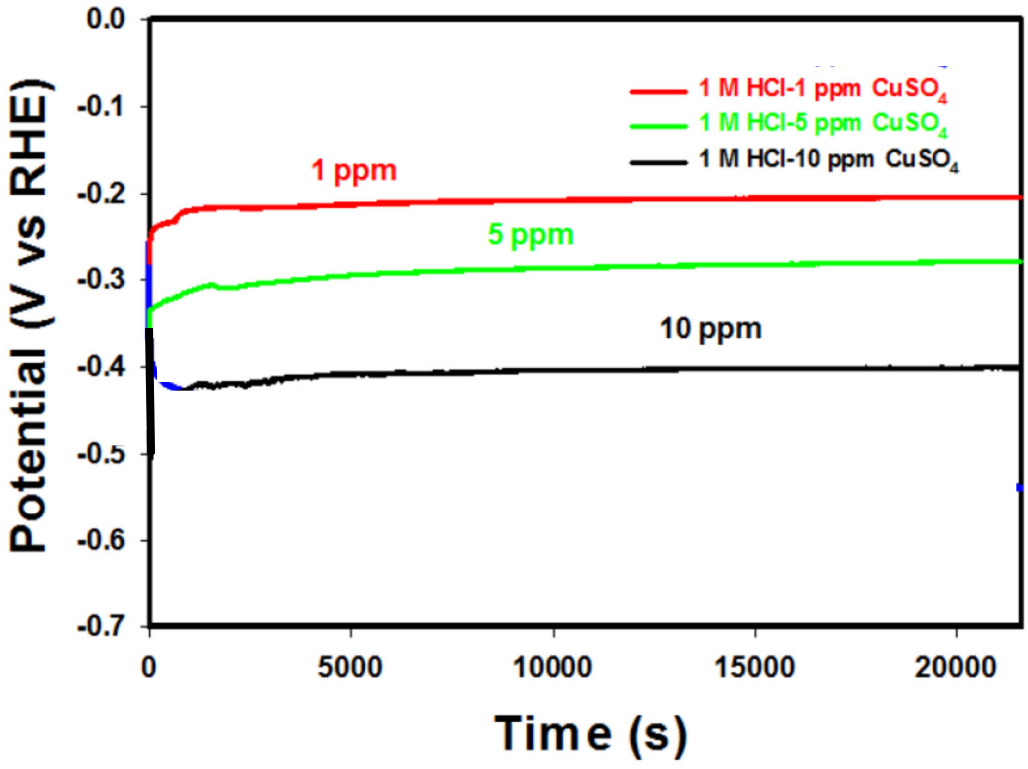

Figure 4.10 Galvanostatic curves at 1.5 A and 25 ℃ obtained during hydrogen production experiments performed in proton pump mode at various [Cu^{2+}] concentrations in 1 M HCl

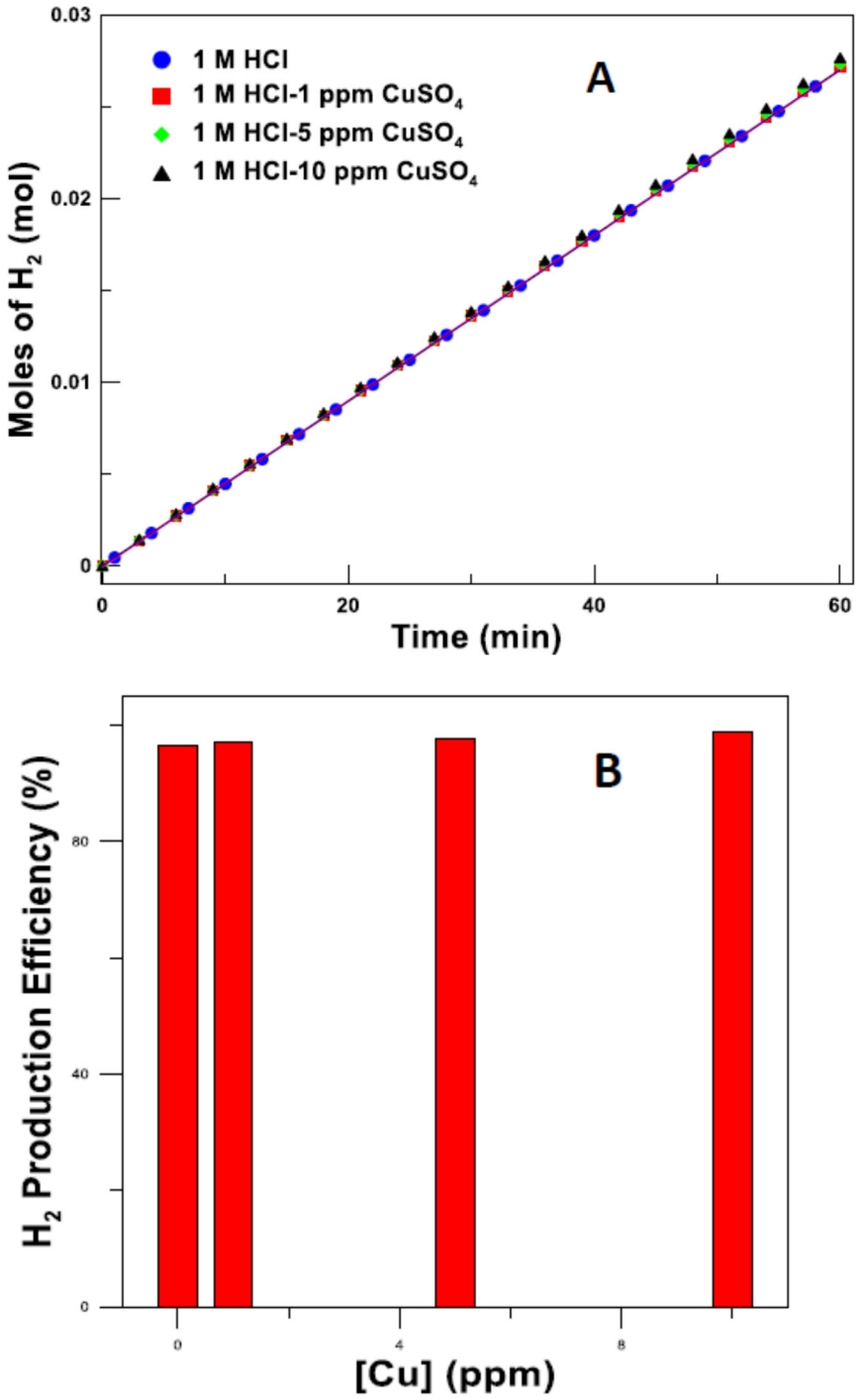

Figure 4.11: A) Moles of H_2 produced as a function of time and B) Hydrogen production efficiency for various copper concentrations at 25 ℃

4.4 Summary

In this chapter a novel proton pump configuration was employed with the catholyte being either H_2SO_4 or HCl spiked with various amounts of copper contaminant. A variety of electrochemical tests were performed in order to determine the effect on both the Coulombic and voltage efficiency associated with HER. UV visible spectroscopy was utilized to determine the speciation of the copper-chloro complexes present in our particular system.

Results obtained in H_2SO_4 show that there is evidence of copper UPD when the $[Cu^{2+}] \leq$ 5 ppm. Once the concentration of copper was raised above this concentration there appears to be a negative impact on the Pt surface health. HER activity was investigated using LSV. These results showed that once the concentration of copper was raised above 5 ppm, there was a dramatic decrease in the observed current density and increase in overpotential. Results from galvanostatic tests show that there is a significant decrease in voltage efficiency with increasing copper concentration, while the Coulombic efficiency remained unaffected. Tests performed in HCl showed that the presence of copper had a negative impact when $[CuSO_4]$ was greater than 5 ppm. HER activity appears to be negatively impacted when the concentration was raised above 5 ppm as well. Galvanostatic tests also showed a similar result as previous tests, with the Coulombic efficiency being unaffected while the voltage efficiency is negatively impacted.

UV-vis results were performed with the concentration of HCl being held constant and the concentration of Cu^{2+} being varied from 0-40 ppm. These copper concentrations are much higher than those used in the electrochemical experiments. It was found that in the absence of copper, there is no notable peak which is to be expected. As the concentration of copper was increased a peak begins to resolve at 250 nm which corresponds to $CuCl^+$. No other peaks are visible. This indicates that this is the only copper-chloro species present at the cathode in our system.

CHAPTER 5: CONCLUSIONS AND FUTURE DIRECTIONS

In this work, the effects of copper contamination at the cathode in Cu-Cl/HCl electrolyzers on the HER reaction was investigated. 3-electrode cell experiments were performed using a planar 3mm planar Pt electrode with varying Cu concentration, chloride concentration and pH. Experiments were first performed in the absence of copper contaminant with the concentration of HCl being varied from 0-1 M. Results showed that there is an increase in the peak current in the hydrogen adsorption/desorption region. CV tests performed with variable copper at a constant pH and chloride concentration show a peak occurring near 0.8 V that increases with increasing copper concentration. This indicates that the presence of copper is detectible at concentrations as low as 1 ppm. There was no significant effect on the e peaks present in the hydrogen adsorption/desorption region of the voltammograms indicating that there was little to no effect on the Pt surface health due to the presence of copper in solution as the peak size/shape remains unchanged. To determine the importance of the presence of chloride, tests were performed in a chloride free media. It was found that the copper was detectable once the concentration was raised above 5 ppm, as indicated by the peak that begins to develop at 0.8 V_{RHE}.

The same tests were performed using a 3 mm GC electrode coated with a 20% Pt/C ink to better represent the surface of the electrode employed in the full cell. Probing the system in the positive potential regime showed that by increasing the surface area of the electrode by adding the Pt/C ink caused the effects of copper on the system to be much less dramatic. This is due to not only the increase in surface area, but the increase in capacitive current caused by the carbon support.

Full cell experiments were performed in proton pump mode. This method employs a dynamic hydrogen electrode in place of the anode. This allows for the Pt surface health to be examined by running in the positive potential regime and the HER kinetics by scanning to negative

potentials. Electrochemical tests were performed at copper concentrations ranging from 0-10 ppm in either a H_2SO_4 or HCl media.

Tests were performed in the absence of chloride so it was possible to have complete control over the amount of copper ions present at the cathode. It was found that when the concentration of copper (II) is raised from 0-5 ppm there is evidence of copper UPD. When the concentration was further increased to 10 ppm there was a clear depression in the peak current in the hydrogen adsorption/desorption region. This can be attributed to the plating of copper onto the electrode surface effectively resulting in blocking of the Pt active surface atoms. HER activity is also effected by the presence of copper in solution. As the concentration of copper increased, there is a distinct increase in the onset potential for the HER and as well as ta decrease in the efficiency. This was evident from the decrease in current density. Galvanostatic hydrogen collection experiments were performed in order to determine the effect of copper contamination on the hydrogen production efficiency. It was found that when the concentration of copper is increased there is a notable increase in overpotential. The hydrogen production efficiency appeared to remain unchanged regardless of the copper concentration.

The same experiments were performed in HCl. Results of CV tests performed on this system show little to no evidence of copper UPD. Once the concentration of copper was raised above 5 ppm, again there appears to be a depression in the peak current in the hydrogen adsorption/desorption region due to copper plating. LSV tests show that when the concentration of copper is higher than 5 ppm there is a significant decrease in the observed current density and increase in onset potential. Galvanostatic experiments again show that there is a significant impact on the voltage efficiency for the HER as the copper concentration was increased. The Coulombic efficiency remains the same regardless of the amount of copper present.

The results obtained in this work lead to a number of conclusions. The presence of copper does in fact negatively impact the HER kinetics and effects the Pt surface state in both the presence and absence of chloride. The copper concentration appears to have no effect on the Coulombic efficiency of the reaction, which suggest that the copper atoms are not necessarily undergoing a charge transfer reaction, and are adsorbed onto the Pt surface.

The proton-pump configuration employed in this work has potential applications beyond just the determination of copper contaminants for this particular electrolysis system. This method of isolating cathodic contaminants in other PEM electrolysis cell systems. For instance, this method could potential be used to determine the effects of Fe(II/III) in the Fe-Cl thermochemical cycle. If the amount of hydrogen pumped into the anode compartment was carefully monitored, this configuration could also allow for quantitative measurements of hydrogen permeation across a particular membrane material based on the amount of hydrogen gas produced at the cathode that would be monitored via the water displacement apparatus component of this system.

Another potential direction for future work on this research project could be to change the composition of the Pt/C structure. There are a number of different carbon support materials that could be incorporated into the electrode material in place of carbon black. The Pt catalyst could also be altered by employing Pt-alloy catalyst material. The activity of different alloy materials could be tested and the data presented in this document used as a baseline. There are also a number of research groups producing ceramic carbon electrodes which have shown great promise in hydrogen fuel cell devices. These electrode materials could be produced and tested for their effectiveness for the Cu-Cl/HCl thermochemical cycle. Temperature is another parameter that was not examined in the research. In increasing the temperature of the reaction

mixtures you increase reaction rate but, could potentially alter the structure of the Pt catalyst of Pt-alloy catalyst.

REFERENCES

(1) Wang, Z.; Daggupati, V. N.; Marin, G.; Pope, K.; Xiong, Y.; Secnik, E.; Naterer, G. F.; Gabriel, K. S. Towards Integration of Hydrolysis, Decomposition and Electrolysis Processes of the Cu-Cl Thermochemical Water Splitting Cycle. *Int. J. Hydrogen Energy* **2012**, *37* (21), 16557–16569. https://doi.org/10.1016/j.ijhydene.2012.02.172.

(2) Edge, P. S. R.; Easton, E. B. Comparison of Novel Anode Materials for the Production of Hydrogen Using CuCl/HCl Electrolyzers. *ECS Trans.* **2013**, *53* (9), 11–20. https://doi.org/10.1149/05309.0011ecst.

(3) Ishaq, H.; Dincer, I. A Comparative Evaluation of Three Cu[Sbnd]Cl Cycles for Hydrogen Production. *Int. J. Hydrogen Energy* **2019**, *44* (16), 7958–7968. https://doi.org/10.1016/j.ijhydene.2019.01.249.

(4) Orhan, M. F.; Dincer, I.; Naterer, G. F.; Rosen, M. A. Coupling of Copper-Chloride Hybrid Thermochemical Water Splitting Cycle with a Desalination Plant for Hydrogen Production from Nuclear Energy. *Int. J. Hydrogen Energy* **2010**, *35* (4), 1560–1574. https://doi.org/10.1016/j.ijhydene.2009.11.106.

(5) Ursúa, A.; Gandía, L. M.; Sanchis, P. Hydrogen Production from Water Electrolysis: Current Status and Future Trends. *Proc. IEEE* **2012**, *100* (2), 410–426. https://doi.org/10.1109/JPROC.2011.2156750.

(6) Ratlamwala, T. A. H.; Dincer, I. Energy and Exergy Analyses of a Cu-Cl Cycle Based Integrated System for Hydrogen Production. *Chem. Eng. Sci.* **2012**, *84*, 564–573. https://doi.org/10.1016/j.ces.2012.08.052.

(7) Generation, T. S.; Photoelectrolysis, W. *Light , Water , Hydrogen Light , Water , Hydrogen*.

(8) Naterer, G.; Suppiah, S.; Lewis, M.; Gabriel, K.; Dincer, I.; Rosen, M. A.; Fowler, M.; Rizvi, G.; Easton, E. B.; Ikeda, B. M.; et al. Recent Canadian Advances in Nuclear-Based Hydrogen Production and the Thermochemical Cu-Cl Cycle. *Int. J. Hydrogen Energy* **2009**, *34* (7), 2901–2917. https://doi.org/10.1016/j.ijhydene.2009.01.090.

(9) Ferrandon, M. S.; Lewis, M. A.; Alvarez, F.; Shafirovich, E. Hydrolysis of CuCl2 in the Cu-Cl Thermochemical Cycle for Hydrogen Production: Experimental Studies Using a Spray Reactor with an Ultrasonic Atomizer. *Int. J. Hydrogen Energy* **2010**, *35* (5), 1895–1904. https://doi.org/10.1016/j.ijhydene.2009.12.034.

(10) Aghahosseini, S.; Dincer, I.; Naterer, G. F. Integrated Gasification and Cu-Cl Cycle for Trigeneration of Hydrogen, Steam and Electricity. *Int. J. Hydrogen Energy* **2011**, *36* (4), 2845–2854. https://doi.org/10.1016/j.ijhydene.2010.11.078.

(11) Ozbilen, A.; Dincer, I.; Rosen, M. A. Life Cycle Assessment of Hydrogen Production via Thermochemical Water Splitting Using Multi-Step Cu-Cl Cycles. *J. Clean. Prod.* **2012**, *33*, 202–216. https://doi.org/10.1016/j.jclepro.2012.03.035.

(12) Wajda, T.; Gabriel, K. Thermolysis Reactor Scale-up for Pilot Scale Cu–Cl Hybrid Hydrogen Production. *Int. J. Hydrogen Energy* **2019**, *44* (20), 9779–9790. https://doi.org/10.1016/j.ijhydene.2018.11.187.

(13) Millet, P.; Mbemba, N.; Grigoriev, S. A.; Fateev, V. N.; Aukauloo, A.; Etiévant, C. Electrochemical Performances of PEM Water Electrolysis Cells and Perspectives. *Int. J. Hydrogen Energy* **2011**, *36* (6), 4134–4142. https://doi.org/10.1016/j.ijhydene.2010.06.105.

(14) Naterer, G. F.; Suppiah, S.; Stolberg, L.; Lewis, M.; Wang, Z.; Daggupati, V.; Gabriel, K.; Dincer, I.; Rosen, M. A.; Spekkens, P.; et al. Canada's Program on Nuclear Hydrogen Production and the Thermochemical Cu-Cl Cycle. *Int. J. Hydrogen Energy* **2010**, *35* (20), 10905–10926. https://doi.org/10.1016/j.ijhydene.2010.07.087.

(15) Wang, Z. L.; Naterer, G. F.; Gabriel, K. S.; Gravelsins, R.; Daggupati, V. N. Comparison of Different Copper-Chlorine Thermochemical Cycles for Hydrogen Production. *Int. J. Hydrogen Energy* **2009**, *34* (8), 3267–3276. https://doi.org/10.1016/j.ijhydene.2009.02.023.

(16) Ozbilen, A.; Dincer, I.; Rosen, M. A. Environmental Evaluation of Hydrogen Production via Thermochemical Water Splitting Using the Cu-Cl Cycle: A Parametric Study. *Int. J. Hydrogen Energy* **2011**, *36* (16), 9514–9528. https://doi.org/10.1016/j.ijhydene.2011.05.067.

(17) Pope, K.; Wang, Z.; Naterer, G. F. Process Integration of Material Flows of Copper Chlorides in the Thermochemical Cu-Cl Cycle. *Chem. Eng. Res. Des.* **2016**, *109*, 273–281. https://doi.org/10.1016/j.cherd.2015.12.024.

(18) Orhan, M. F.; Dincer, I.; Rosen, M. A. The Oxygen Production Step of a Copper-Chlorine Thermochemical Water Decomposition Cycle for Hydrogen Production: Energy and Exergy Analyses. *Chem. Eng. Sci.* **2009**, *64* (5), 860–869. https://doi.org/10.1016/j.ces.2008.10.047.

(19) Ghandehariun, S.; Rosen, M. A.; Naterer, G. F.; Wang, Z. Pinch Analysis for Recycling Thermal Energy in the Cu-Cl Cycle. *Int. J. Hydrogen Energy* **2012**, *37* (21), 16535–16541. https://doi.org/10.1016/j.ijhydene.2012.06.081.

(20) Welaya, Y. M. A.; El Gohary, M. M.; Ammar, N. R. Steam and Partial Oxidation Reforming Options for Hydrogen Production from Fossil Fuels for PEM Fuel Cells. *Alexandria Eng. J.* **2012**, *51* (2), 69–75. https://doi.org/10.1016/j.aej.2012.03.001.

(21) Mazloomi, S. K.; Sulaiman, N. Influencing Factors of Water Electrolysis Electrical Efficiency. *Renew. Sustain. Energy Rev.* **2012**, *16* (6), 4257–4263. https://doi.org/10.1016/j.rser.2012.03.052.

(22) Wang, M.; Wang, Z.; Gong, X.; Guo, Z. The Intensification Technologies to Water Electrolysis for Hydrogen Production - A Review. *Renew. Sustain. Energy Rev.* **2014**, *29*, 573–588. https://doi.org/10.1016/j.rser.2013.08.090.

(23) Carmo, M.; Fritz, D. L.; Mergel, J.; Stolten, D. A Comprehensive Review on PEM Water Electrolysis. *Int. J. Hydrogen Energy* **2013**, *38* (12), 4901–4934. https://doi.org/10.1016/j.ijhydene.2013.01.151.

(24) Ozbilen, A.; Dincer, I.; Rosen, M. A. Environmental Evaluation of Hydrogen Production via Thermochemical Water Splitting Using the Cu-Cl Cycle: A Parametric Study. *Int. J. Hydrogen Energy* **2011**, *36* (16), 9514–9528. https://doi.org/10.1016/j.ijhydene.2011.05.067.

(25) Balta, M. T.; Dincer, I.; Hepbasli, A. Comparative Assessment of Various Chlorine Family Thermochemical Cycles for Hydrogen Production. *Int. J. Hydrogen Energy* **2016**, *41* (19), 7802–7813. https://doi.org/10.1016/j.ijhydene.2015.12.222.

(26) Farsi, A.; Kayhan, Ö.; Zamfirescu, C.; Dincer, I.; Naterer, G. F. Azeotropic Pressure Swing Distillation of Hydrochloric-Water for Hydrogen Production in the Cu–Cl Cycle: Thermodynamic and Design Methods. *Int. J. Hydrogen Energy* **2019**, *44* (16), 7969–7982.

https://doi.org/10.1016/j.ijhydene.2019.01.048.

(27) Zamfirescu, C.; Naterer, G. F.; Dincer, I. Kinetics Study of the Copper/Hydrochloric Acid Reaction for Thermochemical Hydrogen Production. *Int. J. Hydrogen Energy* **2010**, *35* (10), 4853–4860. https://doi.org/10.1016/j.ijhydene.2009.08.077.

(28) Balta, M. T.; Dincer, I.; Hepbasli, A. Potential Methods for Geothermal-Based Hydrogen Production. *Int. J. Hydrogen Energy* **2010**, *35* (10), 4949–4961. https://doi.org/10.1016/j.ijhydene.2009.09.040.

(29) Naterer, G. F.; Suppiah, S.; Rosen, M. A.; Gabriel, K.; Dincer, I.; Jianu, O. A.; Wang, Z.; Easton, E. B.; Ikeda, B. M.; Rizvi, G.; et al. Advances in Unit Operations and Materials for the Cu–Cl Cycle of Hydrogen Production. *Int. J. Hydrogen Energy* **2017**, *42* (24), 15708–15723. https://doi.org/10.1016/j.ijhydene.2017.03.133.

(30) Wang, Z. L.; Naterer, G. F.; Gabriel, K. S.; Gravelsins, R.; Daggupati, V. N. New Cu-Cl Thermochemical Cycle for Hydrogen Production with Reduced Excess Steam Requirements. *Int. J. Green Energy* **2009**, *6* (6), 616–626. https://doi.org/10.1080/15435070903364731.

(31) Orhan, M. F.; Dincer, I.; Rosen, M. A. Design of Systems for Hydrogen Production Based on the Cu-Cl Thermochemical Water Decomposition Cycle: Configurations and Performance. *Int. J. Hydrogen Energy* **2011**, *36* (17), 11309–11320. https://doi.org/10.1016/j.ijhydene.2011.02.034.

(32) Ranganathan, S.; Edge, P. S.; Easton, E. B. Evaluation of Anode Electrode Materials for Cu-Cl/HCl Electrolyzers for Hydrogen Production; 2012; Vol. 41, pp 111–120. https://doi.org/10.1149/1.3702861.

(33) Abdo, N.; Bradley Easton, E. Nafion/Polyaniline Composite Membranes for Hydrogen Production in the Cu-Cl Thermochemical Cycle. *Int. J. Hydrogen Energy* **2016**, *41* (19), 7892–7903. https://doi.org/10.1016/j.ijhydene.2015.11.180.

(34) Duarte, M. V.; Lozano-Sanchez, P.; Katakis, I. Copper UPD as Non-Specific Adsorption Barrier in Electrochemical Displacement Immunosensors. *Biosens. Bioelectron.* **2009**, *24* (7), 2205–2210. https://doi.org/10.1016/j.bios.2008.11.032.

(35) Bin, Z. "Solid Oxide Fuel Cell (SOFC) Technical Challenges and Solutions from Nano-Aspects." *Int. J. energy Res.* **2009**, *31* (August 2007), 135–147. https://doi.org/10.1002/er.

(36) Lam, A.; Li, H.; Zhang, S.; Wang, H.; Wilkinson, D. P.; Wessel, S.; Cheng, T. T. H. Ex Situ Study of Chloride Contamination on Carbon Supported Pt Catalyst. *J. Power Sources* **2012**, *205*, 235–238. https://doi.org/10.1016/j.jpowsour.2012.01.063.

(37) Marković, N. M.; Gasteiger, H. A.; Lucas, C. A.; Tidswell, I. M.; Ross, P. N. The Effect of Chloride on the Underpotential Deposition of Copper on Pt(111): AES, LEED, RRDE, and X-Ray Scattering Studies. *Surf. Sci.* **1995**, *335* (C), 91–100. https://doi.org/10.1016/0039-6028(95)00452-1.

(38) Oviedo, O. A.; Vélez, P.; MacAgno, V. A.; Leiva, E. P. M. Underpotential Deposition: From Planar Surfaces to Nanoparticles. *Surf. Sci.* **2015**, *631*, 23–34. https://doi.org/10.1016/j.susc.2014.08.020.

(39) Uchikoshi, M. Determination of the Distribution of Cobalt-Chloro Complexes in Hydrochloric Acid Solutions at 298 K. *J. Solution Chem.* **2018**, *47* (12), 2021–2038. https://doi.org/10.1007/s10953-018-0831-z.